FINAL REPORT
U.S. Department of Energy

Optimization of Thermochemical, Kinetic, and Electrochemical Factors Governing Partitioning of Radionuclides during Melt Decontamination of Radioactively Contaminated Stainless Steel

Principal Investigator

James A. Van Den Avyle
Sandia National Laboratories

Co-Investigators

David Melgaard
Martin Molecke
Greg J. Shelmidine
Sandia National Laboratories
Albuquerque, NM

Prof. Uday Pal
Department of Manufacturing Engineering
Boston University
Boston, MA

Sergie. I. Bychkov
Scientific Technology Center, Mining & Chemical Combine
Zheleznogorsk, Russia

Contributors

W.P. Chernicoff and C.J. MacDonald (BU)
M. Eric Schlienger, James Stepanek and Rodney Williamson (SNL)
K.G. Kudinov, Sergie Podoynitsin, and Vasily V. Zhidkov (STC)

Project Number: 60603
Project Duration: (FY96-FY99)

Table of Contents | Page

I. Executive Summary 4

II. Research Objectives 6

III. Methods and Results 7

1. ESR Slag Properties and Slag-Surrogate Interactions 7

- **A. The Electroslag Remelting Process** 8
- **B. Slag Solubility Study** 9
- **C. Slag Volatilization Study** 11
- **D. Slag Viscosity Study** 14
- **E. Slag Surface Tension Measurements** 15
- **F. Slag Electrical Conductivity Experiments** 15
- **G. Slag-Metal Partition Experiments** 19
- **H. Conclusions** 23

2. ESR Decontamination Melting using Surrogates 24

- **A. Electroslag Remelting Decontamination** 24
- **B. Surrogate Chemistry Selections** 25
- **C. Laboratory Experimental Design** 27
- **D. Ingot Analysis** 29
- **E. Slag Analysis** 33
- **F. Conclusions** 35

3. ESR Experiments with Radionuclides 37

- **A. Contaminated Electrode Design and Fabrication** 37
- **B. Selection of the Refining Slag** 38
- **C. Melting and Sampling Procedure** 39
- **D. Analytical Techniques** 42
- **E. Discussion of Results** 42
- **F. Conclusions** 47

IV. Relevance, Impact, and Technology Transfer **49**

V. Project Productivity **49**

VI. Personnel Supported/Associated **49**

VII. Publications **50**

VIII. Interactions **51**

IX. Transitions **52**

X. Patents **52**

XI. Future Work **52**

XII. Literature Cited **53**

I. Executive Summary

This research addresses the melt decontamination of radioactively contaminated stainless steel by electroslag remelting (ESR). ESR is industrially used for the production of specialty steels and superalloys to remove a variety of contaminates and to improve metal chemistry. Correctly applied, it could maintain the specified chemistry and mechanical properties of the original material while capturing the radioactive transuranic elements in a stable slag phase. The ESR process also produces a high quality metal ingot free of porosity that can be directly forged or rolled into final shapes.

The goal of this project was to optimize a melt decontamination process through a basic understanding of the factors which govern the partitioning of various radionuclides between the metal, slag, and gas phases. Radionuclides which are captured by a slag phase may be stabilized by promoting the formation of synthetic minerals within a leach resistant matrix. This research program included three segments. At Boston University, Prof. Uday Pal and his group conducted research to develop a fundamental understanding of thermochemical and electrochemical behaviors of slag/metal/radionuclide surrogate systems. This work combined experimental characterization and thermochemical modeling of these high temperature systems. The second segment utilized Sandia expertise and ongoing work in fundamental separation science and liquid metal processing technology to investigate and optimize ESR decontamination using representative surrogate compounds to represent contaminate radionuclides. This work evaluated partitioning of the surrogates between the slag and metal ingot in ESR experiments. Furnace operating parameters were systematically varied to determine the optimum slag processing conditions. The third effort in Russia conducted ESR melting experiments using contaminated stainless steel pipe electrodes doped with plutonium. This work provided separation data for the radioactive compounds.

At Boston University, it was shown that the ESR base slag (60wt%CaF_2-20wt%CaO-20wt%Al_2O_3) has a high capacity to incorporate CeO_2 (surrogate for Pu and U oxides). The equilibrium partition ratio for the Ce (surrogate for U and Pu) between the metal and slag phases was determined as a function of temperature. The partition ratio was on the order of 10^{-4}, and it decreased as the temperature increased. Sr (surrogate for radioactive Sr) was soluble in the slag (up to 1 w%). Relatively high Hf concentrations were

observed in the metal phase (100 ppm range); this may indicate a limited hafnia solubility or a high hafnia activity in the slag.

Slag physical properties including interfacial tension, and viscosity were determined. The slag volatilization rate was measured as a function of temperature and was observed to follow an Arrhenius behavior. The electrical conductivity of the base slag was measured as a function of temperature using two methods. They both show an Arrhenius behavior indicating that the conduction mechanism does not change in the measured temperature range.

At Sandia, several experimental melts using surrogate elements, Ce, Cs, Hf, Re and Sr to simulate the reactions of several common radioactive contaminants, were conducted in an ESR furnace. The amount of the surrogates far exceeded the expected amounts of true decontamination melts. Even with these large amounts, the ESR process generally proved highly effective in keeping all the surrogates, except for Re, from the resulting stainless steel ingot, either by transporting them into the slag or by volatilization. Generally, all the Re, Ce and Hf could be accounted for in the slag or in the metal. However, significant portions of the Cs and Sr were unaccounted for and were presumed to have volatilized. The Re was used as the chemical homologue for the important fission product, ^{99}Tc. Based on this study, ESR using the chosen slag compositions would not be appropriate for decontamination of technetium. However, all the surrogates for Pu and U were effectively transported from the metal, so the ESR can be recommended for decontamination of these elements.

At the M&CC in Russia, it was shown that ESR results in stainless steel deactivation of plutonium-239, cesium-137, americium-241 and europium-152 with high purification factors. At the same time, purification of such radionuclides as cobalt-60 and niobium-94 practically did not occur.

The purified stainless steel was high quality, with a uniform distribution of residual contaminations and main alloying components, satisfactory structural and mechanical properties, and absence of defects and inclusions, especially when re-melted with the slag 70 %CaF_2 + 30 % Al_2O_3. The product could be reused as steel 08C18N10 (the USA analogue is steel 302 per AISI) to fabricate equipment utilized in nuclear applications.

II. Research Objectives

Metal waste generated from domestic nuclear operations for defense and commercial applications has led to a growing stockpile of radioactively contaminated scrap metal, much of which is stainless steel. This steel contains large quantities of strategic elements such as nickel and chromium and constitutes a valuable domestic resource [1]. A significant fraction of this material cannot be efficiently surface decontaminated, and burial of this material would be wasteful and expensive, since long term monitoring would be necessary in order to minimize environmental risk. Melt decontamination of this material would maintain the chemical pedigree of the stainless steel, allowing its controlled reuse within the nuclear community.

This research addresses the melt decontamination of radioactively contaminated stainless steel by electroslag remelting (ESR). ESR is industrially used for the production of specialty steels and superalloys to remove a variety of contaminates and to improve metal chemistry. Correctly applied, it could maintain the specified chemistry and mechanical properties of the original material while capturing the radioactive transuranic elements in a stable slag phase. The ESR process also produces a high quality metal ingot free of porosity that can be directly forged or rolled into final shapes.

The goal of this project was to optimize a melt decontamination process through a basic understanding of the factors which govern the partitioning of various radionuclides between the metal, slag, and gas phases. Radionuclides which are captured by a slag phase may be stabilized by promoting the formation of synthetic minerals within a leach resistant matrix. This research program included three segments. At Boston University, Prof. Uday Pal and his group conducted research to develop a fundamental understanding of thermochemical and electrochemical behaviors of slag/metal/radionuclide surrogate systems. This work combined experimental characterization and thermochemical modeling of these high temperature systems. The second segment utilized Sandia expertise and ongoing work in fundamental separation science and liquid metal processing technology to investigate and optimize ESR decontamination using representative surrogate compounds to represent contaminate radionuclides. This work evaluated partitioning of the surrogates between the slag and metal ingot in ESR experiments. Furnace operating parameters were systematically varied to determine the optimum slag processing conditions. The third effort in Russia conducted ESR melting experiments using contaminated stainless steel pipe electrodes doped with plutonium. This work provided separation data for the radioactive compounds.

III. Methods and Results

1. ESR Slag Properties and Slag-Surrogate Interactions

At Boston University, Prof. Uday Pal and his group conducted research to develop a fundamental understanding of thermochemical and electrochemical behaviors of slag/metal/radionuclide surrogate systems. This work combined experimental characterization and thermochemical modeling of these high temperature systems. Goals were 1) to measure and characterize equilibrium partition functions of the surrogate contaminants between the slag and the metal as a function of the temperature and atmosphere 2) to measure and characterize slag physical properties including electronic conductivity, viscosity, surface tension, and volatilization in air as a function of temperature. A laboratory facility was set up to perform these high temperature measurements. Significant effort went into to development of the necessary crucibles, electrochemical cell configuration, and other experimental techniques for high temperature measurements in the corrosive fluoride containing molten slags used in ESR.

This research program investigated the decontamination of stainless steel (radioactive scrap metal, or RSM) using the ESR process by conducting thermochemical and thermophysical studies on the ESR slag (60wt.% CaF_2–20wt.% CaO–20wt.% Al_2O_3). The radioactive contaminants of interest are oxides of uranium (U), plutonium (Pu), and strontium (Sr). The nonradioactive surrogates used to simulate and test these radioactive contaminants in the laboratory are oxides of Ce and Hf (for U and Pu oxides), and Sr (for its radioactive counterpart).

The thermochemical studies include measurement of the solubility of the surrogate oxides in the slag, the partition coefficient of the surrogate between the slag and the metal as a function of temperature, and thermodynamic modeling of the activities of the slag constituents as a function of temperature. The solubility and the partition coefficient measurements illustrate the quantitative ability of the slag to remove the contaminants and the thermodynamic activity modeling provides a general framework to predict other thermophysical and thermochemical properties such as viscosity, surface tension, volatilization and reactivity. The thermophysical studies include measurement of the electrical conductivity (κ) for the ESR slag. The electrical conductivity is measured with a novel high-accuracy-height-differential technique that requires no calibration. This method consists of making continuous AC impedance measurements over several successive depth increments of the coaxial cylindrical electrodes in the ESR slag. The electrical conductivity is then calculated from the slope of the plot of inverse impedance versus the depth of the electrodes in the slag. The measured volatilization rate and the volatile species of the ESR slag indicate that the ESR slag composition essentially remains the same during the duration of the electrical conductivity measurements. This technique has been employed to investigate the changes in the electrical conductivity of the ESR slag as a function of the temperature and the amounts of the surrogate oxides that are typically incorporated in the ESR slag.

A. The Electroslag Remelting (ESR) Process

In the ESR process (Figure 1), the RSM forms one of the two electrodes. Joule heating through a molten slag layer maintains the slag temperature between 1700-2000°C and melts one end of the RSM electrode. The molten metal droplets from the consumable (RSM) electrode fall through the slag layer. While the metal is in contact with the slag, most of the radioactive contaminants from the metal are preferentially incorporated into the slag. The metal droplets are solidified in a water-cooled copper mold and form part of the consolidated and decontaminated ingot underneath the slag layer. This can be easily formed into a useful product by mechanical processes such as rolling, forging, etc. The ingot also serves as the other electrode in the process. The slag containing the contaminants is removed as a solid and can be reused or appropriately disposed.

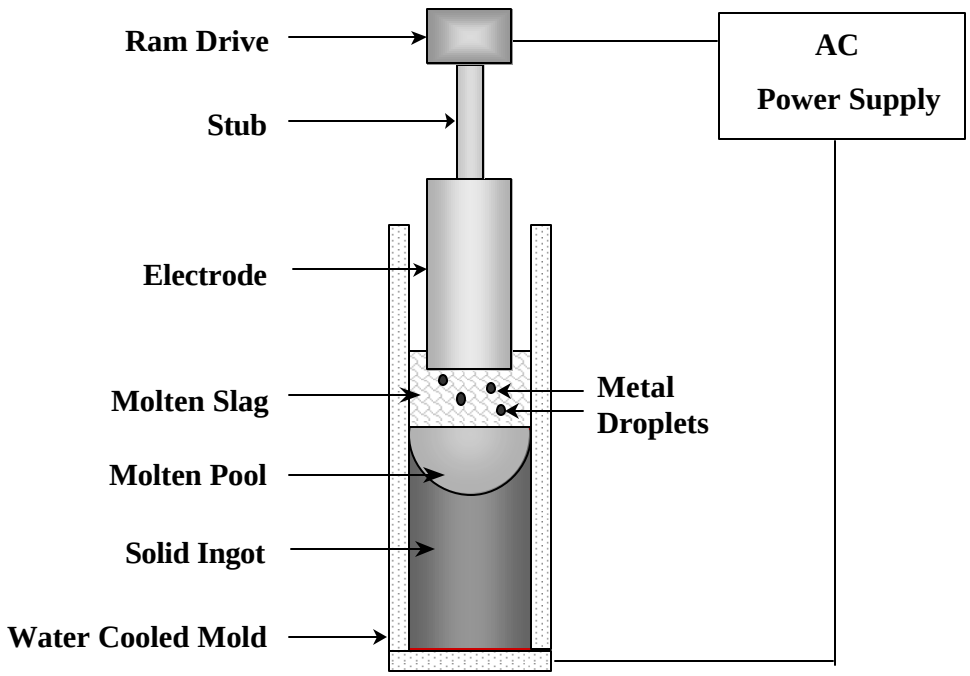

Figure 1: ESR Process

The slag in the ESR process is crucial for its success [2]. For instance, it must have a low partition ratio for the contaminants between the metal and the slag. This will allow most of the contaminant to be incorporated in the slag phase. Its interfacial properties must be such that it wets the metal for effective removal of the contaminants, but it must not facilitate formation of slag skin around the ingot. It is desirable to minimize the slag skin around the ingot and concentrate the radioactive contaminants in the slag cap over the ingot. Along with surface tension, its density and viscosity must be such that it provides sufficient residence time for the metal droplets without adversely affecting slag fluidity and mass-transfer properties. The electrical conductivity must be such that it

provides efficient joule heating. A high melt rate of the RSM would result in a high production rate, however this condition would not necessarily optimize the end product (recycled stainless steel) in the ESR process [3]. Conversely, a very low melt rate in the ESR process causes the solidified ingot to have coarse crystalline grains and poor surface finish. Hence, an accurate knowledge of the ESR slag conductivity may be essential for establishing a control strategy for obtaining the desired melt rate in the ESR process. The electrical conductivity of the slag may be used as one of the input parameters in the ESR process control model. The volatilization rate and the volatile species in the ESR process must be known in order to determine compositional variations of the slag and the associated electrical conductivity changes during the ESR process, and to establish an effective means of capture for the volatile species, if necessary. The solid-state slag structure must be such that the phases formed are stable and non leachable to accommodate easy handling and disposal.

The ESR base slag investigated in this research program is 60wt%CaF_2-20wt%CaO-20wt%Al_2O_3. Preliminary ESR trials have shown that this slag can be used to decontaminate radionuclides and chemical surrogates from contaminated stainless steel [4]. However, the ability of the slag to remove the contaminants has not been quantified. It is desirable to know the partition coefficient of the contaminant between the slag and the metal in order to fully understand the capabilities and limitations of the slag to sufficiently clean the RSM. In this research program, the potential radioactive contaminants of interest to be removed from the stainless steel are uranium (U), plutonium (Pu), cesium (Cs), strontium (Sr) and technetium (Tc). Due to high oxygen affinity of U, Pu, Cs, Sr and Tc, these radioactive contaminants are expected to be present as oxides in decommissioned nuclear processing, fabrication and nuclear reactor facilities either as surface contaminants or lodged in cracks and crevices of piping or other components. The nonradioactive surrogates used to simulate and test these radioactive contaminants are oxides of Ce and Hf (for U and Pu oxides), Re (for Tc oxide) and Cs and Sr (for their radioactive counterparts).

The ESR slag that is investigated here is 60wt%CaF_2-20wt%CaO-20wt%Al_2O_3 with and without xCeO_2 (CeO_2 is the nonradioactive surrogate for U and Pu oxides); 'x' varying from 250ppm to 25wt%. The investigation conducted includes measurements of CeO_2 solubility in the slag, slag-metal partition coefficient for Ce, slag volatilization, viscosity, electrical conductivity and surface tension. The measurements were made primarily between 1400-1650°C and were extrapolated to higher temperatures by utilizing the Arrhenius relationship.

` B. Slag Solubility Study

Experiments were conducted in an open-air induction furnace by melting and equilibrating 10g of either base slag (60wt%CaF_2-20wt%CaO-20wt%Al_2O_3) or 10g of base slag mixed with different amounts of ceria (Table II). The experimental setup is schematically shown in Figure 2. The base slag was prepared by self-milling the constituent powders. The ceria (produced by sol-gel) was sintered in air at 1695°C to a

theoretical density of over 90% as a closed-porosity pellet. Portions of the ceria pellet were broken and added to the slag as needed. The slag samples were all isothermally held at 1500°C for 15 minutes and air quenched. This process was determined to be adequate for equilibrating the molten slag.

Mass of Base Slag (g)	Mass of CeO_2 (g)	Weight Percent of CeO_2	Results of Air Quenched (from 1500°C)
10.000	0.000	0.00	2-phase structure
10.155	0.0025	0.025	2-phase structure
9.973	0.010	0.10	2-phase structure
10.065	0.051	0.50	2-phase structure
10.010	0.105	1.00	2-phase structure
10.000	0.254	2.50	2-phase structure
10.060	0.495	4.70	2-phase structure
10.907	0.990	8.30	3-phase structure
10.028	1.510	13.10	3-phase structure
10.031	2.996	23.00	3-phase structure

Table I: Details of the Solubility Experiments

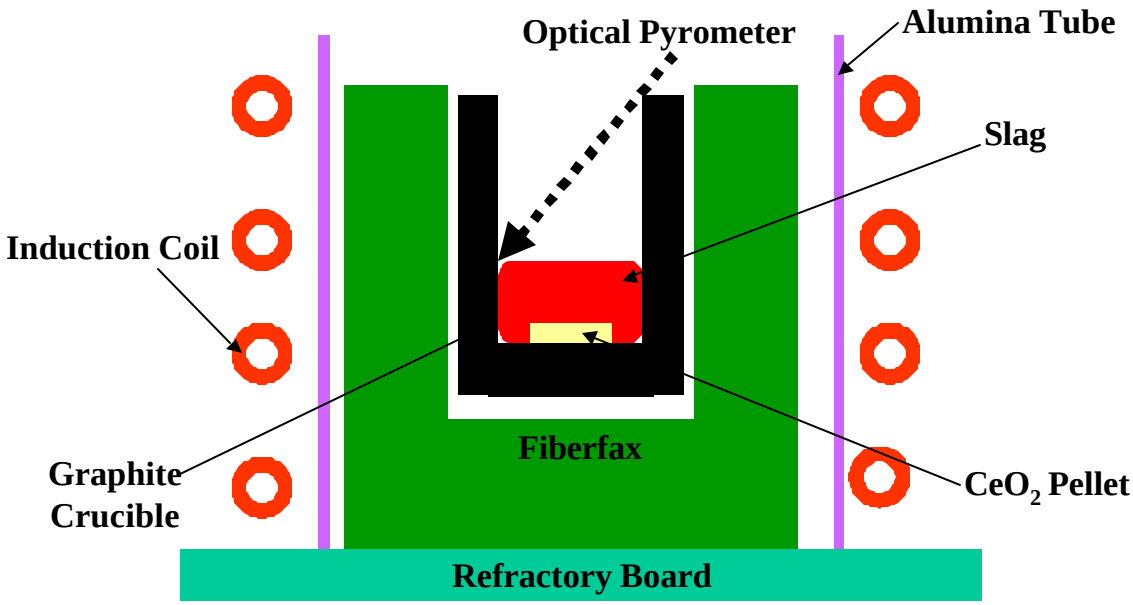

Figure 2: Experimental Setup for CeO_2 Solubility Study

The quenched graphite crucible was sectioned along the central axis with a low speed diamond saw using an oil lubricant. The sample was cleaned with methanol and mounted either in an acrylic or epoxy medium. The sample was polished with diamond paste and cleaned during the process with methanol.

The polished samples were analyzed with Electron Micro Probe (EMP) JEOL SuperProbe 7300. Wavelength Dispersed Spectroscopy was used for the chemical analysis; the standards used are shown in Table II. A light element detector was used for the fluorine and oxygen analysis. Image analysis was used to determine the fraction of each type of phase present. By combining the image analysis with the composition analysis of the phases, a comparison was made between the analyzed and theoretical composition of the slag.

Element	F	Ce	Al	Ca	O
Standard	CaF_2	$CePO_4$	Al_2O_3	$CaAl_2SiO_8$	Al_2O_3

Table II: Standards Used in EMP Analysis

EMP analyses showed that the air-quenched base slag is homogeneous and has a two-phase structure, one is darker than the other. The dark phase contained Al-Ca-O-F. If we assume that the fluorine is associated with Ca as CaF_2, then the remaining Al-Ca-O had a composition that closely matched $5CaO\text{-}3Al_2O_3$. The lighter phase contained Ca-F and its composition matched CaF_2. The dark-colored phase (Al-Ca-O-F), solidified first, and the Ca-F phase, which is the light colored phase, solidified later. These observations agree with the expected crystallization path of the slag [5]. When CeO_2 was added to the slag up to 4.7wt%, the air-quenched slag still had the same two-phase structure. The higher melting Al-Ca-O-F phase had a higher concentration of Ce in solid solution, and the Ca-F phase had a much lower concentration of Ce. It is interesting to note that when the CeO_2 content is 2.5wt% or more in the base slag, the backscattered electron image of the Al-Ca-O-F phase with Ce in solid solution changes from dark to light. This is due to the variable Ce content. When the CeO_2 content was 8.3wt% or more, there appeared a third crystalline Ce-rich phase that grew in size as the CeO_2 content increased. However, these high CeO_2 levels may not be interest to the ESR decontamination process, because the level of CeO_2 in the slag phase is not expected to exceed a couple 1000ppm.

The foregoing observations have profound implication on the slag-metal partition coefficient. Since the CeO_2 is completely soluble in the ESR slag (60wt%CaF_2-20wt%CaO-20wt%Al_2O_3), it implies that the CeO_2 activity in the ESR slag will be extremely small since its concentration is not expected to exceed 2000 ppm. Therefore, from the Ce/CeO_2 equilibrium, it is reasonable to expect that the Ce concentration in the metal phase will be below the detection limit (<1ppm).

C. Slag Volatilization Study

The purpose of the study is to determine the rate at which the base slag and the base slag mixed with different amounts of ceria volatilizes as a function of temperature and the chemical nature of the volatile species. This is accomplished using a thermogravimetric (TG) balance and a quadropole mass analyzer. Also the volatile species were condensed and chemically analyzed.

The TG balance used was a CAHN D-100 Series system that is run with CAHN D-100 Series software version 2.0. The experiments are conducted in a graphite crucible suspended in a purified argon atmosphere to prevent oxidation of the crucible material. The arrangement is schematically shown in Figure 3. In order to measure the volatilization rate of the slag with CeO_2, it was necessary to reduce the CeO_2 to Ce_2O_3 prior to melting the slag so that the vaporization rate could be attributed to slag volatilization instead of CeO_2 reduction; under the experimental conditions maintained in the TG experiments Ce_2O_3 was the stable phase. TG results with base slag and base slag with ceria are shown in Table III with the calculated evaporation rates. The natural logarithm of the evaporation rate as a function of inverse temperature for the runs reported in Table III are shown in Figure 4. From Figure 4, it can be seen that the volatilization rate of the base slag and the base slag with ceria did not differ much and followed an Arrhenius behavior. The volatilization rate of the base slag as a function of temperature can be expressed as:

$$R = 3445.26\exp(-\frac{37955.09}{T})$$

The experimental setup used to condense the volatile slag species onto a water-cooled copper coil is shown in Figure 5. The condensed vapor was an amorphous powder. Therefore, in order to analyze by X-ray diffraction, an attempt was made to crystallize the powder by annealing at 1000°C. The diffraction pattern showed the presence of CaF_2 . In order to determine the uncondensed volatile species, the volatile gas from the base slag was passed through a quadropole mass analyzer. The spectra from the mass analyzer showed presence of AlF_3 among the volatile species.

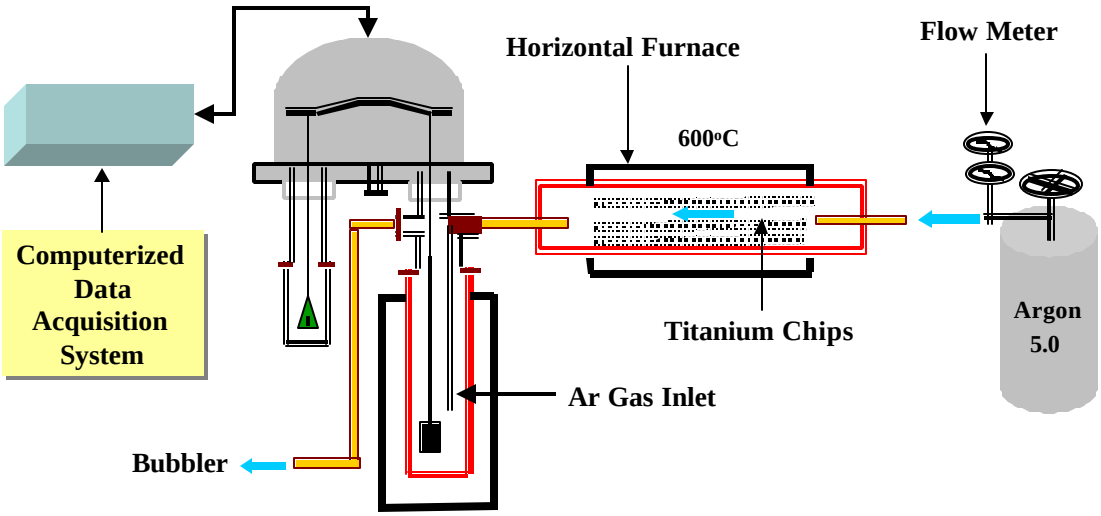

Figure 3: Thermogravimetry Experimental Setup to Study Volatilization

Experiment Type	Base Slag Mass (g)	CeO_2 Mass (g)	Temperature (^oC)	Volatilization Rate (g/cm2-sec.)
Pure Base Slag	37.687		1450	1.010E-06
Pure Base Slag	37.687		1500	1.500E-06
Pure Base Slag	37.687		1550	3.280E-06
Pure Base Slag	37.687		1600	5.560E-06
100ppm Ceria	38.017	0.00382	1450	1.378E-06
100ppm Ceria	38.017	0.00382	1500	1.892E-06
100ppm Ceria	38.017	0.00382	1550	3.313E-06
100ppm Ceria	38.017	0.00382	1600	4.958E-06
40000ppm Ceria	36.009	1.440	1450	7.006E-07
40000ppm Ceria	36.009	1.440	1500	2.193E-06
40000ppm Ceria	36.009	1.440	1550	4.001E-06
40000ppm Ceria	36.009	1.440	1600	6.286E-06
100000ppm Ceria	34.896	3.4896	1450	8.921E-07
100000ppm Ceria	34.896	3.4896	1500	2.318E-06
100000ppm Ceria	34.896	3.4896	1550	4.002E-06
100000ppm Ceria	34.896	3.4896	1590	5.965E-06

Table III: Thermogravimetric Experiments and Results

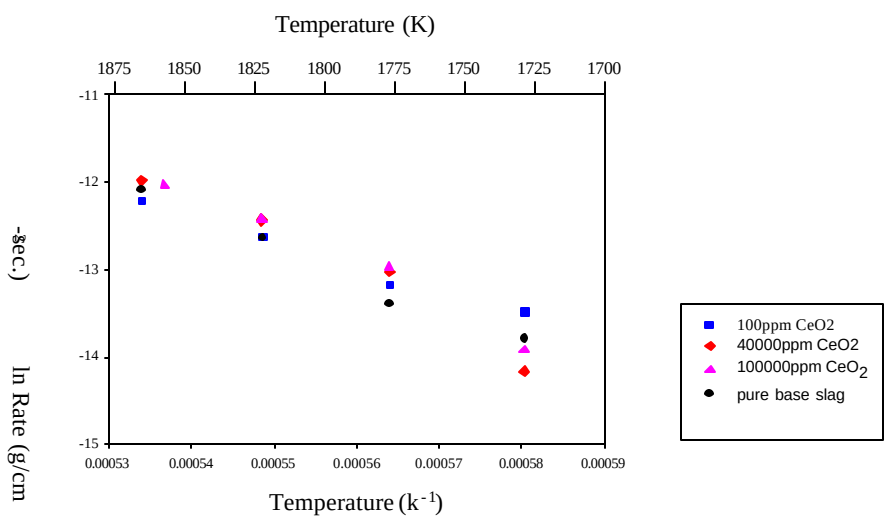

Figure 4: Comparison of Results of Volatilization Experiments

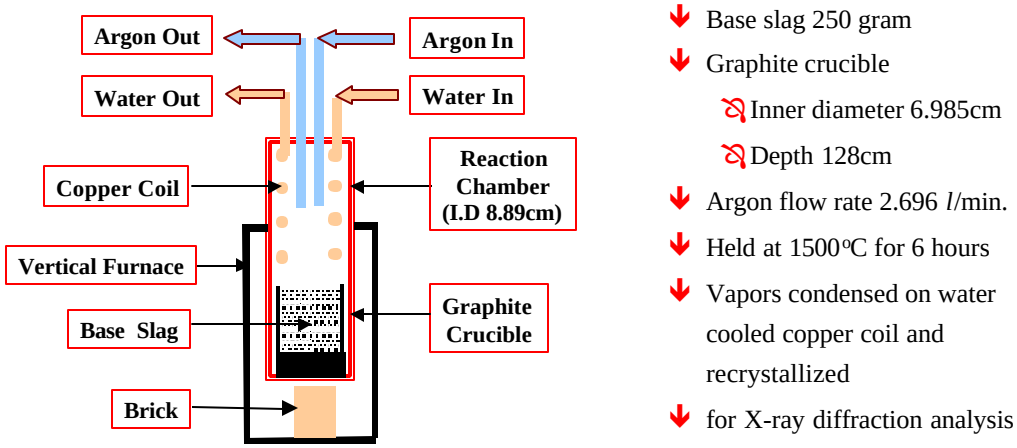

Figure 5: Experimental Setup for Identification of Volatile Species

D. Slag Viscosity Study

The viscosity of the base slag was measured using an inner cylinder rotation technique. The schematic of the set up is shown in Figure 6. The viscosity measurements were conducted as a function of temperature. The results are shown in Table IV and plotted in Figure 7. From Figure 7, it is apparent that there is a drastic increase in the viscosity of the base slag as the temperature decreases from 1400°C to 1390°C. This means that the base slag does not remain as a single phase below 1390°C. This conclusion is consistent with the liquidus temperature of the base [5]. Furthermore, above 1400°C the viscosity is not a strong function of the temperature indicating that the slag is fluid and does not have long polymeric chains. The measured volatilization rate is not significant to change the fluorine content of the slag during the ESR process and therefore the slag viscosity is not expected to change.

Temperature (k)	Viscocit (dPa.s)
1500	0.868
1500	0.707
1450	0.748
1400	0.708
1390	7.461
1380	6.806
1370	19.301

Table IV: Base Slag Viscosity as a Function of temperature

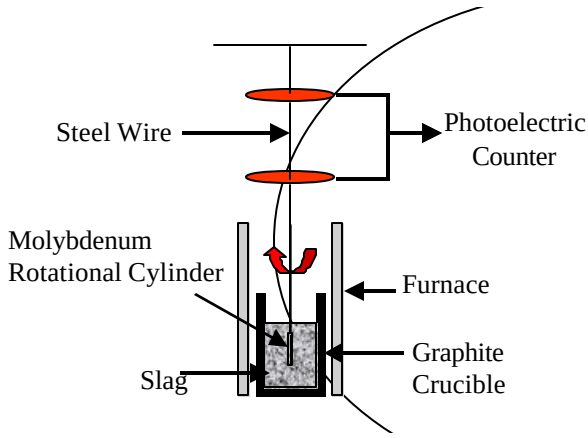

Figure 6: Setup for Viscosity Measurement

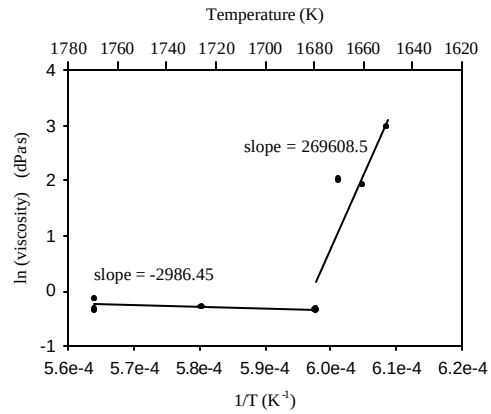

Figure 7: Arrhenius Plot of Base Slag Viscosity

E. Slag Surface Tension Measurements

The slag surface tension measurements were made using the maximum bubble pressure method over a temperature range of 1400-1460°C. The schematic of the set up is shown in Figure 8. The measurements were made as a function of temperature. The results are plotted in Figure 9. Figure 9 shows that the surface tension of the molten slag follows an Arrhenius behavior.

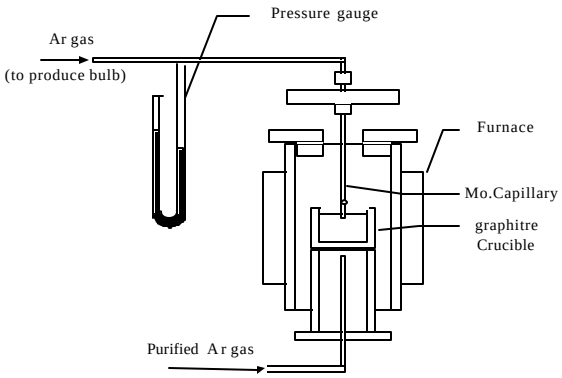

Figure 8: Set up for Surface Tension

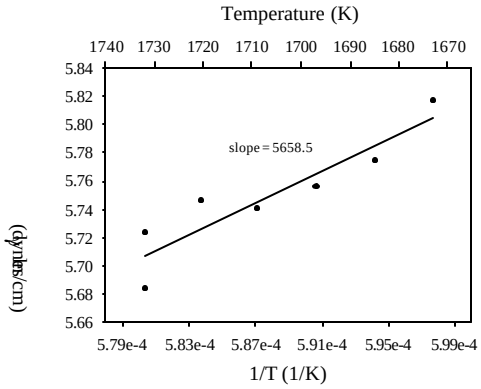

Figure 9: Arrhenius Plot of Base Slag Surface Tension

F. Slag Electrical Conductivity Measurements

The electrical conductivity was first measured using a less precise AC impedance method with 2-point electrodes, as shown in Figure 10. The cell constant was determined by measuring the electrical conductivity of a KCl standard solution at 25°C. The electrical conductivity of the base slag was measured as a function of temperature. The single Arrhenius behavior (Figure 11) above and below the single-phase region (around 1390°C) indicates that the conduction mechanism remains primarily unchanged, probably dominated by the F ions.

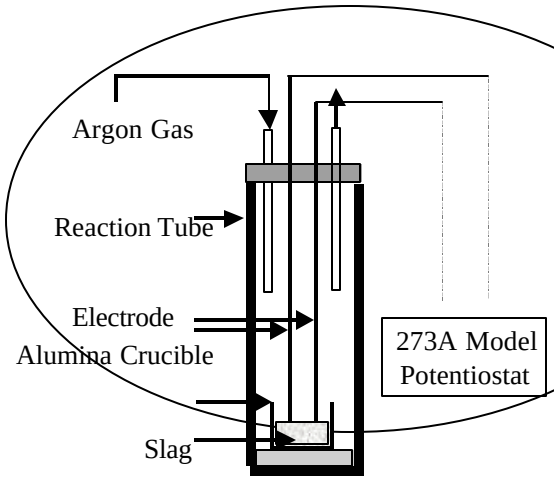

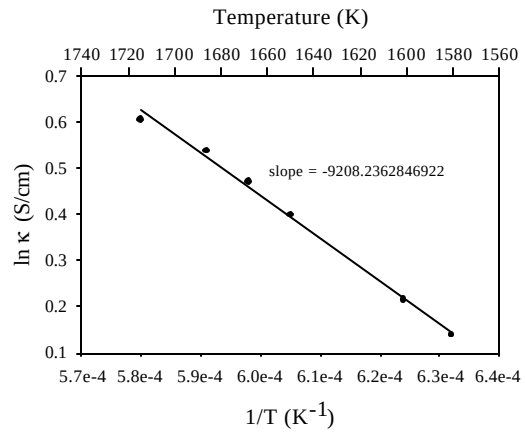

Figure 10: Set up of Electrical Conductivity Figure 11: Arrhenius Plot of Conductivity

A novel calibration free conductivity cell was developed that measures the molten slag impedance as a function of electrode height. The electrodes are coaxial and symmetrical as shown in Figure 12. From the slope of the linear plot of slag impedance as a function of the depth of electrode immersed, the slag conductivity is calculated. This technique is significantly more accurate then the 2-point method.

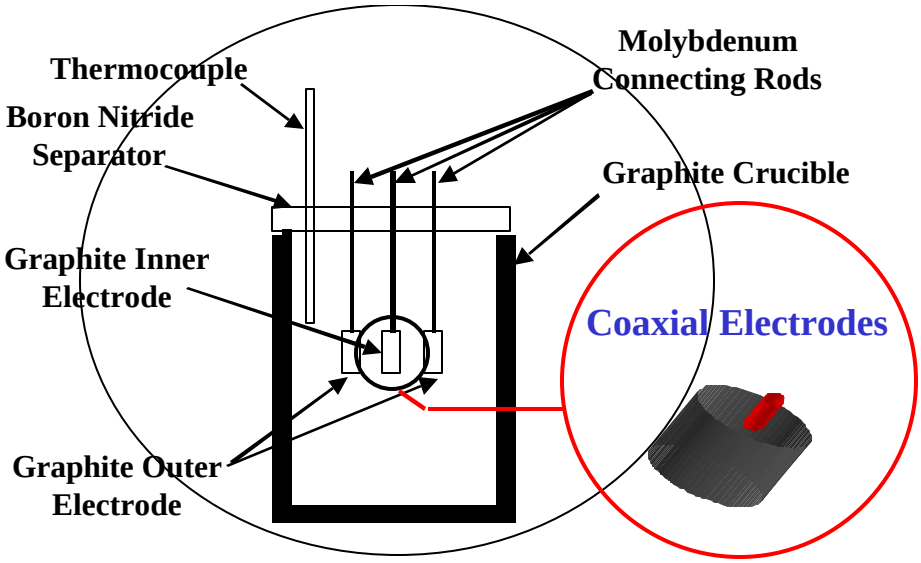

Figure 12: Calibration-free Conductivity Cell

Approximately one kilogram of base slag was packed in a graphite crucible (8.26 cm OD x 7.62 cm ID) for each experimental run. The graphite crucible with the base slag was lowered into a vertical tube furnace. The electrochemical cell (Figure 13) consists of a graphite cylinder (3.18 cm ID) serving as the outer electrode and a graphite rod (6.35 mm OD) serving as the inner electrode. The amount of base slag was approximately 8.26 cm high when melted.

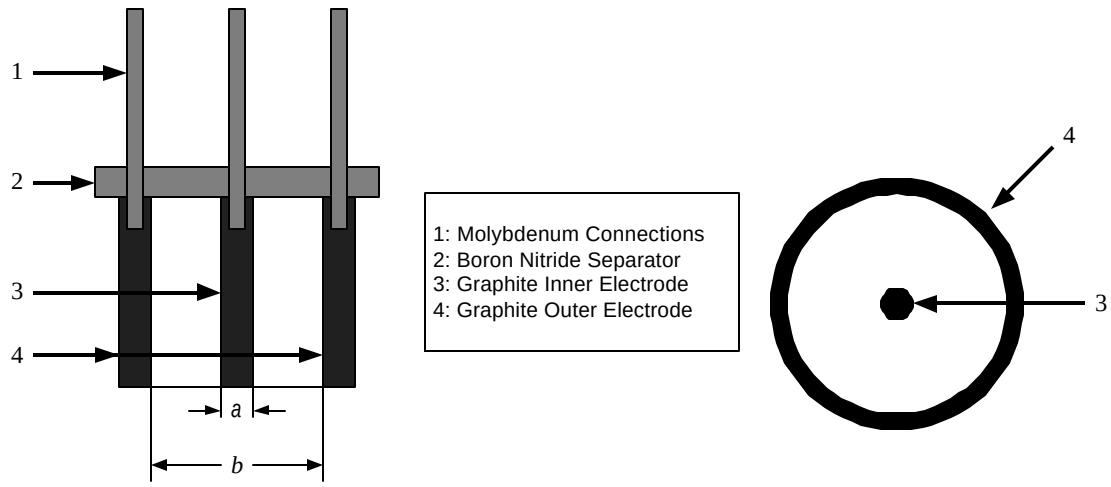

Figure 13: Electrochemical Cell for High-Accuracy-Differential-Height Technique

Typically, electrical conductivity measurements of the base slag were made at three different temperatures in one experimental run, going from the highest to the lowest temperature. The electrodes are lowered by increments of 0.254 mm by the digital micrometer and the AC impedance scans are repeated for each depth increment. These measurements are made for a total of 21 successive depth increments. This is sufficient statistically to determine the slope for the plot of inverse impedance ($1/Z_{sol'n}$) versus depth (z). The high-accuracy-height-differential conductivity measurement technique requires no calibration. Continuous AC impedance measurements are taken over a wide frequency range for each successive depth increment of a coaxial cylindrical electrode system in the slag. From these measurements, the impedance of the solution is acquired for each depth increment [6], the inverse impedance of the solution ($1/Z_{sol'n}$) is plotted versus the corresponding depth. The slope of the straight line in this plot is used for calculating the electrical conductivity (K) of the base slag.

There are some critical advantages to the high-accuracy-height-differential technique that permits its applicability for measuring the electrical conductivity of the base slag. Due to the concentricity and the rigid shape of the electrodes, the current travels through a well-defined path. Since the cell constant is inversely proportional to the immersed depth of the coaxial cylindrical electrodes in the slag, there is no need for the high-accuracy-height-differential technique to be calibrated. Another advantage is that the measurements are possible at high temperatures because the (arbitrary) initial immersion of the electrodes does not require the exact surface to be known or visible. Therefore, the measurements can be made in a furnace at high temperatures where the base slag solution is obstructed from one's view.

A typical experimental run of the base slag, which consists of making measurements at three different temperatures (1550, 1500, and 1460°C), results in a plot of the inverse impedance of the solution versus the depth increments for each temperature as shown in Figures 14 (example for 1550°C). The slope from this linear plot is used to calculate the electrical conductivity (κ) of the base slag at the specific temperature. The electrical

conductivity measurements from the high-accuracy-height-differential technique showed a single Arrhenius behavior for the base slag as shown in Figure 15. The Arrhenius equation based on linear regression is:

$$\ln k = 6.593 - \frac{10175}{T}$$

where κ is the electrical conductivity in S/cm and T is the temperature in Kelvin. The Arrhenius behavior indicates that the conduction mechanism remains primarily unchanged; the conduction mechanism is most likely dominated by the F ions.

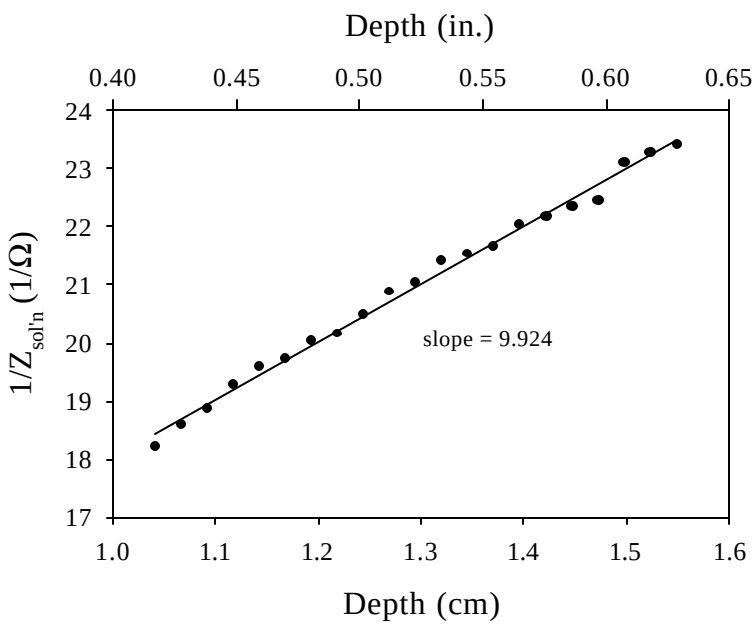

Figure 14: Plot of Inverse Impedance versus Depth at 1550°C

The Arrhenius behaviors of the ESR base slag, measured by the high-accuracy-height-differential technique, reported in the Slag Atlas [7], and measured last year using the less accurate 2-point probe technique, are plotted in Figure 15. These plots show nearly identical trends for the high-accuracy-differential-height technique and the Slag Atlas, while the baseline measurement appears to be lower and parallel to the high-accuracy-height-differential technique. Since the baseline measurement utilized a two-point electrodes method, the measured cell constant introduces a source of error. The very similar Arrhenius behavior for the ESR base slag as measured by the high-accuracy-height-differential technique and as reported in the Slag Atlas is reasonable since each method employs a similar cell geometry. Even though these techniques both have well defined current paths, the high-accuracy-height-differential technique is calibration free and therefore quicker and easier to conduct.

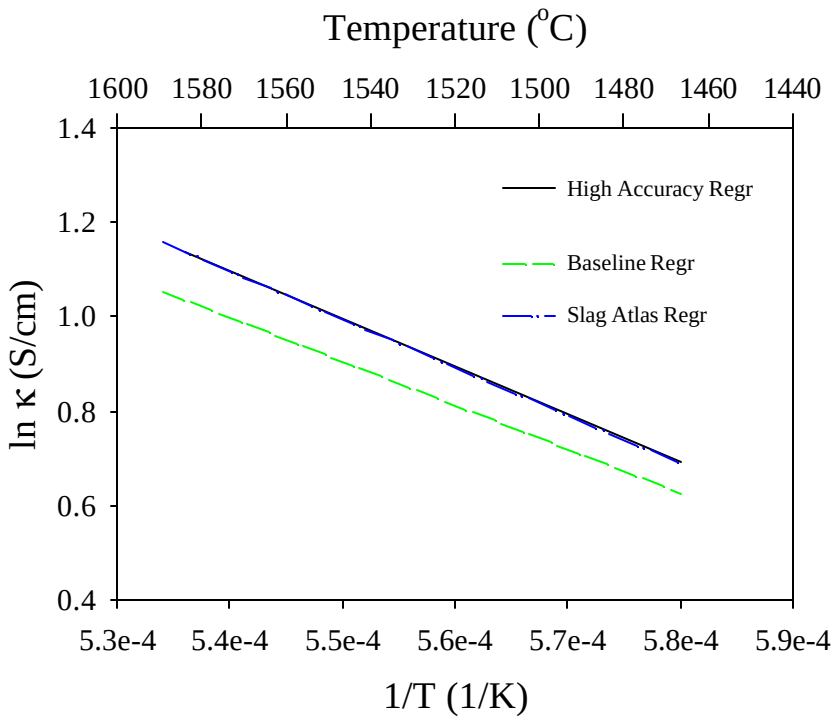

Figure 15: Arrhenius Plot Comparison of Different Techniques

Attempts were made to measure the electrical conductivity of the base slag with separate additions of the surrogate oxide (CeO_2) for the radioactive contaminants (uranium and plutonium) and the surface enhancer TiO_2. Unfortunately, the conditions in the conductivity-cell chamber were such that the added oxides formed carbides along the graphite conductivity cell that lowered the measured value of the electrical conductivity. It is anticipated that the semiconducting nature of ceria (CeO_2) and titania (TiO_2) could alter the electrical conductivity of the base slag. If this can be accurately measured, then it can be used as a sensing parameter to measure the incorporation of the contaminant or the surface enhancer in the ESR slag and also serve as one of the input parameters for the ESR process control.

G. Slag-Metal Partition Experiments

A total of 88 experiments were conducted with hafnia and strontia surrogates. Carbon-saturated iron used in these experiments to fix the oxygen activity in the metal. The base slag components were 60wt% CaF_2 – 20wt% CaO – 20wt% Al_2O_3. All experiments were carried out in an open-air induction furnace. Experiments conducted with the hafnia and strontia surrogates were at 1500, 1600, 1650 and 1700°C and those with the ceria surrogates were at 1600, 1650, and 1700°C. At each temperature and for each surrogate type, four concentrations of the surrogate in the base slag were used; approximately 1wt%, 0.5 wt%, 0.25 wt%, and 0.05 wt%. Fifteen grams of the slag and 0.6-0.85 grams of carbon-saturated iron were used in each experiment.

With each concentration of the surrogate in the base slag, two separate experiments were conducted at a given temperature, one with a 15 minute hold to equilibrate the slag followed by a 15 minute hold with the metal in the slag, and the other with a 15 minute hold to equilibrate the slag followed by a 30 minute hold with the metal in the slag. All experiments were conducted in graphite crucibles, and all samples were air quenched in the crucible. The atmosphere over the slag during the experiment was essentially a CO(g) environment resulting from the oxidation of the graphite crucible and the oxygen partial pressure over the slag was much lower than in air. Under these conditions, thermodynamic data indicates that the surrogate will dissolve in the slag as an oxide. This was confirmed from the slag analysis after the experiments; no carbon containing phases were found.

Slag samples were analyzed using XRF and electron-microprobe equipped with a WDS analyzer. The metal samples were analyzed using laser ablative–inductively coupled plasma – mass spectrometer. (LA-ICP-MS). Analysis of the slag was performed at MIT, Department of Geology using the electron-microprobe, and Department of Materials Science and Engineering using the Spectro Corp Quantitative XRF. The analysis showed that the surrogate oxides, ceria and strontia, were completely dissolved and homogeneous at concentrations used in these experiments. However, the slag containing 1 w% hafnia had a different quenched phase structure compared to the 1 w% ceria or the 1 w% strontia slags. An inhomogeneous distribution of a hafnium-rich phase was observed. This suggested that hafnia incorporation in the slag is very different from that of ceria or the strontia. In fact, in ESR slag with ceria, ceria-rich phases formed only when the ceria concentration in the slag exceeded 8 w%. This may suggest that hafnia has a higher activity or lower solubility in the slag as compared to the ceria surrogate.

Analysis of the metal was performed at the Harvard University, Department of Planetary Sciences, using their LA-ICP-MS. The LA-ICP-MS offers several advantages over other analytical techniques. The machine is capable of analyzing in the ppb range, and offers excellent accuracy in the 1 to 0.1 ppm range. Several samples were mounted in a single ring and rough polished. The analysis of each ring was preceded and followed by running a standard. The detection limit of the LA-ICP-MS for the surrogate elements in iron is around 0.03 ppm.

<u>Slag with Ceria Surrogate</u>: The partition function is defined as the concentration of Ce in the metal divided by the concentration of Ce in the slag. Graphs of the Ce concentration in the metal versus the Ce concentration in the slag at each temperature (1600, 1650 and 1700°C) are linear, indicating that thermodynamic equilibrium was achieved (an example is Figure 16 at 1650°C).

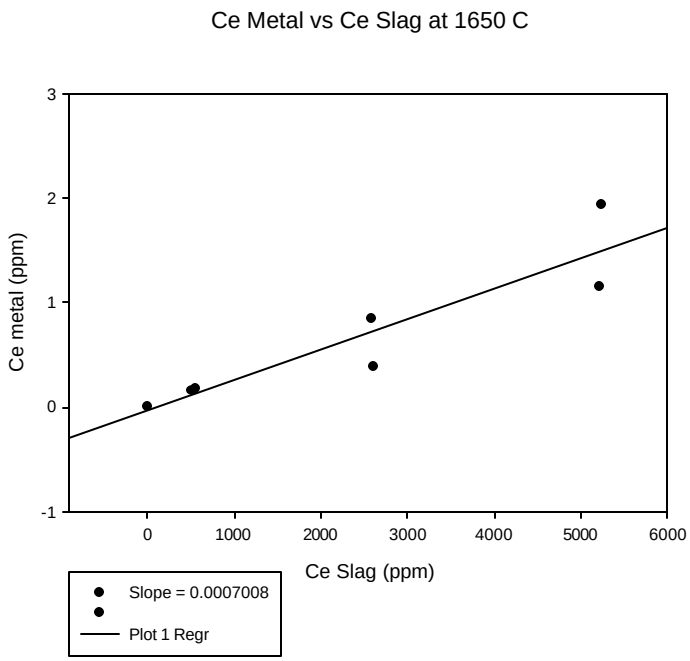

Figure 16: Cerium Distribution between Metal and Slag at 1650°C

The data indicates a decrease in the cerium partition ratio with increasing temperature (Figure 17). Over the temperature range studied, the partition ratio is on the order of 10^{-4}. This indicates that during the ESR operation at temperatures higher than those studied in this investigation and under more oxidizing atmospheres, the slag-metal partitioning of the contaminant will be more effective. For instance, with an initial contamination on the order of 100ppm in the RSM, the residual contaminant in the initially decontaminated ingot will be less than 0.01 ppm, and during the final stages of the run when the contaminant concentration in the slag rises to around 1000 ppm, the residual contaminant in the decontaminated ingot will be less than 0.1 ppm. The study is in agreement with previous work done by Buckentin who found that in actual ESR operations, the surrogate concentration in the decontaminated RSM was below the detectable 1ppm level. Thus, one can conclude that the ESR base slag has a good capability for sufficiently removing the contaminants analogous to ceria from the RSM.

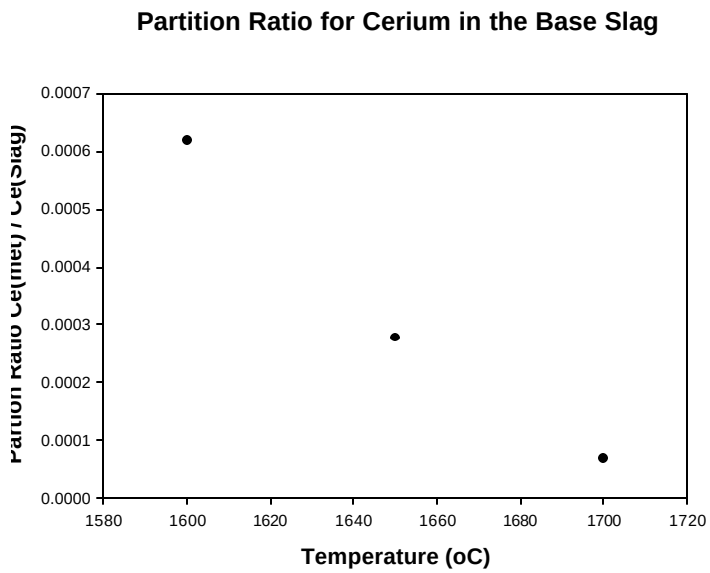

Figure 17: Cerium Partition Ratio between Metal and Slag as a Function of Temperature

Slag with Strontia Surrogate: Sr concentrations in the metal versus the Sr concentration in the slag, at each of the four temperatures (1500, 1600, 1650 and 1700°C), were measured. Independent of temperature and Sr concentration in the slag, the Sr concentration in the metal ranged from 0.5 to 1.5 ppm (within the scatter in the data). There appears to be a solubility limit for Sr (approx. 1 ppm range) in the metal. This observation is also consistent with the fact that, at all the temperatures investigated, the partition ratio of Sr decreased asymptotically with increase in Sr concentration in the slag as per the mass-balance criteria.

Slag with Hafnia Surrogate: Hf concentrations in the metal versus the Hf concentration in the slag were determined at each of the four temperatures (1500, 1600, 1650 and 1700°C). At all temperatures investigated, there was no clear trend in the variation of Hf concentration in the metal or the partition ratio, versus the Hf concentration in the slag. As per the metal analysis, there is a large variation in the Hf concentration in the metal and some of the reported concentrations are in the 100 ppm range. The metal analysis was reviewed and it was found that the spectra analyzed for Hf was not consistent. It was noted from the slag analysis that the 1 w% hafnia-containing slag had a different structure as compared to the 1 w% ceria slag. It is possible that the hafnia activity in the slag is larger than that of ceria at the same concentration level or the slag has lower solubility for hafnia or the slag was not completely homogeneous. It is very likely that the equilibrium Hf concentration in the metal may be an order of magnitude higher than that of Ce.

H. Conclusions

It was shown that the ESR base slag (60wt%CaF_2-20wt%CaO-20wt%Al_2O_3) has a high capacity to incorporate CeO_2 (surrogate for Pu and U oxides). The equilibrium partition for the Ce (surrogate for U and Pu) between the metal and slag phases were determined as a function of temperature. The partition ratio was on the order of 10^{-4}, and it decreased as the temperature increased. Sr (surrogate for radioactive Sr) had a limited solubility in the metal phase (approximately 1 ppm). Ceria and strontia were soluble in the slag (upto 1 w%) and the slag was homogeneous. Air quenched slag structure did not show any isolated high ceria or strontia containing phases. However, no clear trend was observed for the Hf (surrogate for U and Pu) partition between the metal and the slag phases. Relatively high Hf concentrations were observed in the metal phase (100 ppm range). The air quenched hafnia-containing slag (with 1 w% hafnia) showed isolated pockets of Hf-rich phase in the slag. This structure was clearly different from the ceria-containing and Sr-containing slags. This may indicate a limited hafnia solubility or a high hafnia activity in the slag.

The interfacial tension, viscosity, and solidification behavior of the base slag were determined. The slag volatilization rate was measured as a function of temperature and was observed to follow an Arrhenius behavior. The slag volatilization rate was found to be low, and the ceria surrogate, when incorporated in the slag did not significantly alter the volatilization rate. The volatile species were found to be primarily CaF_2 and AlF_3. The electrical conductivity of the base slag was measured as a function of temperature using a less accurate 2-probe method. It also followed an Arrhenius behavior indicating that the conduction mechanism does not change in the measured temperature range.

The high-accuracy-height-differential technique provided an effective method for measuring the electrical conductivity of highly conductive melts, such as the ESR slag, because of the increased electrochemical cell geometry and the capability to make smaller high precision depth increments. The height-differential part of this technique permits the measurements to be made without prior calibration of the cell constant on a similarly conductive solution at high temperatures. Thus, the high-accuracy-height-differential technique eliminates the critical and time consuming step of measuring the cell constant that is present in the traditional electrical conductivity measurement methods. The electrical conductivity of the base slag was measured and followed an Arrhenius behavior. The measured values of the electrical conductivity were compared with those found in literature.

2. ESR Decontamination Melting using Surrogates

A. Electroslag Remelting Decontamination

The major objective for this ESR decontamination study was to evaluate the decontamination capacity or partitioning effectiveness of the ESR process on stainless steel for several major radioactive species, through the use of nonradioactive, surrogate testing at Sandia National Laboratories (SNL). Much of the background work for surrogate chemistry selection was previously compiled and documented by Buckentin in her Ph.D. thesis [1]. A series of eight laboratory melts were conducted to evaluate the effectiveness of using the electroslag remelting (ESR) process to transport radionuclides from the liquid metal phase to the liquid flux or slag phase. To determine the decontamination effectiveness, several surrogate compounds for uranium, plutonium and other fission products were added to the melts. During the melts, the melting rate was varied, typical slag additives were used, and two different slag compositions were evaluated. The resultant post-test ingots and slag were then analyzed to determine the partitioning of the surrogates.

The ESR process shown in Figure 1 was designed to melt the metal electrode into a mold that is slightly larger than the original piece of metal. Typically AC power is applied to the electrode and passes though the slag to the molten metal below the slag. The slag has by far the greatest impedance in the circuit, so it is resistively heated by the current (3 to 5 KA on our furnace but much more on industrial furnaces) passing through the furnace to a temperature above the melting point of the metal. The electrode then melts, coalescing into droplets on the bottom that then fall through the slag and collect in a pool in the mold. As the electrode melts, the ram drive is employed to translate the electrode downward to keep its end immersed in the slag. The mold is water cooled to extract the heat from the molten metal, causing it to solidify. Since the slag is also in contact with the cool mold, a small quantity of slag solidifies against the mold and remains there while the ingot forms inside the mold. This quantity of slag is referred to as the slag skin. The skin serves as a thermal and electrical insulator for the process and is an important factor in the surface quality of the ingot and also in the formation of slag inclusions on the side of the ingot. The slag skin is significant in this study since it may contain some of the contaminating elements. Typically the skin detaches and falls to the floor as the mold is removed but under adverse conditions may adhere to the ingot surface or be entrapped in the ingot. Clearly these conditions need to be avoided for decontamination. Various slag additives and melting conditions have been used to this end. For more information on ESR see the references [8-10].

Because of the slag's reactive properties, the chemistry of the electrode can be altered to meet the specifications for a particular alloy. This alteration takes the form of either removing undesirable elements or adding particular elements. A large variety of different slag compositions are used in ESR depending on the alloys being produced and the types of reactions needed. The details of these compositions are beyond the scope of this report (see [11-13]). The ones recommended by Buckentin [1] for decontamination were used

for this investigation. The important sites for chemical reactions and transport of elements between the slag and the metal are 1) the surface of the electrode immersed into the slag (ideally about 5 mm), 2) the droplets as they fall through the slag and 3) the surface of the molten pool. Important to the kinetics of the reaction at each site are the ratio of the slag to metal volume and the time the two materials remain in contact. The electrode surface has a large slag-to-molten metal volume ratio and a longer contact time than the droplets. The droplets have a large volume ratio as well but short duration from perhaps a few seconds to fractions of a second. On the other hand, the pool has a lower slag-to-metal volume ratio and, depending on the densities of metal and the other elements, may have a long or a short contact time.

B. Surrogate Chemistry Selections

Isotopes of uranium, plutonium, technetium, strontium, cesium are the major radioactive species expected for contaminated metals in nuclear processing, fabrication or reactor facilities. These contaminants are expected to be present predominantly as various oxides either as particulate surface contaminants or lodged in cracks or crevices of piping or other components. Table V summarizes the properties of interest for stainless steel, the major slag components (calcium fluoride, calcia and alumina), and the slag additive titanium dioxide. The table lists if known, the density at room temperature, melting point, boiling point and element electronegativity values. At the ESR operating temperature (~1800-2000°C), the chemical species present in the melt may be different, as determined by previous and ongoing thermodynamic modeling. Also noted are the properties for U and Pu, for metals, oxides, and fluorides credibly present in decontamination ESR melts. Other U and Pu species that could be present at the high temperatures are not listed. For the purposes of surrogate recommendations they were not considered. In previous studies, nonradioactive Ce, Nd and La had been used as chemical homologues, instead of U and Pu. Buckentin used the oxides CeO_2, La_2O_3 and Nd_2O_3. We used only CeO_2 as a useful U and Pu surrogate for simplicity since the other oxides are quite similar to CeO_2 in terms of chemical properties, density and element electronegativity (see Table V). We also used HfO_2 as a second U and Pu (as well as a Th) surrogate, since it has a higher density (greater than liquid steel) and closer to that of UO_2, and an electronegativity value closer to that of Pu (as compared to that of La, Nd or Ce). HfO_2 has previously been used as a PuO_2 surrogate in a Japanese pilot-scale ESR study.[14,15]

For the other fission products different surrogates were included. Nonradioactive Sr (as SrO) and Cs (as Cs_2O) can be used instead of radioactive ^{90}Sr and ^{132}Cs contaminants on metal components. There are no nonradioactive species of technetium. Therefore, we used Re (as ReO_2) as the chemical homologue for the important fission product, ^{99}Tc. The suggested fission product surrogate compounds are noted with an asterisk (*) in Table V. At the high temperatures in the ESR slag melt, it was expected that some of the species will be volatilized, while most strontium species, as well as Re (metal), would not be volatilized and were expected to be captured in the melt. Although many of the fission product surrogate compounds are volatile, their inclusion lent credibility to the end results.

Properties of Slag, Radioactive and Surrogate Compounds						
Compound	**Atomic Weight / Use**	**density**	**Melting Point °C**	**Boiling Point °C**	**Oxide States**	**Electronegativity**
Fe (stainless)	56	7.87	1535			1.83
CaF_2	slag	3.18	1423	~2500		1.00 Ca
CaO	slag	3.3	2614	2850		
Al_2O_3	slag	3.97	2015	2980		1.61 Al
TiO_2	additive	4.26	1830	2500-3000		1.54 Ti
Al	27	2.7	660	2057	+3	1.61 Al
U	238	19.05	1132	3818	+3,4,5,6	1.38
UO_2*	270	10.96	2878			
U_2O_8	842	8.3	d. 1300 (>UO_2)			
UF_3	295		d.<1000			
UF_4	314	6.7	960	1480		
UF_6	352	4.68	64.5	56.2		
Pu	239.1	16.5-17.7	122-639		+3,4,5,6	1.28
PuO_2*	271.1	11.46	2400			
PuF_3	296.1	9.32	1425			
PuF_4	315.1	7	1037	sublimes		
PuF_6	353		50.8	62.3		
Ce	140.1	6.66	799	3426	+3,4	1.12
CeO_2*	172.1	7.13	2600			
Ce_2O_3	328.4	6.86	1692			
CeF_3	197.1	6.16	1460	2300		
Hf	178.5	13.31	2227	4602	+4	1.3
HfO_2*	210.5	9.68	2812			
La_2O_3	325.8	6.51	2307	4200	+3	1.10 La
Nd_2O_3	336.5	7.24	2272		+3	1.14 Nd
Sr	87.6	2.6	769	1384	+2	0.95
SrO*	103.6	4.7	2430			
SrF_2	125.6	4.24	1473	2489		
Cs	132.9	1.88	28.4	669	+1	0.79
Cs_2O*	281.8	4.25	d. 400 (>Cs)			
CsF	151.9	4.12	682	1251		
Re	186.2	20.53	3180	5627	+4,6,7	1.9
ReO_2*	218.2	11.4	d. 1000 > Re		(Tc simulant; > 1.36)	
Re_2O_7	484.4	6.1	~297	subl. 250		

Table V: Properties of Slag, Radioactive and Surrogate Compounds

The specified oxides were added to the melts to approximate 100 ppm (parts per million) concentrations in the ingot for all the surrogate chemical species except for CeO_2. Since the electrodes were approximately 100 kg, 10 g of each of the five surrogate oxides were used. That is considered an obviously large amount of each contaminant, presuming it was a radioactive U or Pu species, and a massive overtest amount for fission product species.

Using 5 kg of slag, the starting 100 ppm becomes concentrated to about 2000 ppm or 0.2%, which was easily analyzed post-test. To evaluate the chemical, physical and thermal effects of surrogate (or actual radioactive) species on high slag loadings, CeO_2 was added at the higher concentration of 1,000 ppm. This made analysis for any residual Ce species transferred to the end melt ingot somewhat easier. It also provided for continuity with the ESR melts conducted earlier by Buckentin [1], who used concentrations of 1,000 to 10,000 ppm. Such high levels of contaminants of actual radioactive species may be considered to be excessively high, but are useful in experimental validation of the ESR process.

With the exception of the HfO_2, all the surrogate species powders were blended and then poured and packed into 0.6 cm (1/4") stainless steel thin walled tubing with an inside diameter of 0.3 cm ~(1/8"). The tubes were attached to the electrodes along their circumferences. The tubing had ~1 cm crimps approximately every 7.6 cm. These insured that the surrogates would be added gradually over the course of the melt. The type C (W-Re) thermocouples (TCs) used to measure the slag temperature each contained ~2.8 g of HfO_2. As the four TCs dissolved approximately 11.2 grams were added, so no additional quantity was needed. Using this procedure caused the Hf to be added in relatively large quantities periodically providing an additional element of over testing. The ingots were cut to sample the portion of the metal where the TCs dissolved.

C. Laboratory Experimental Design

The experimental design for the melts at Sandia National Laboratories consisted of eight melts. The melts used several melting rates designed to span the range of low to high melting rates on the furnace, two common slag additives, and two different slag chemistries. The variations in melting rate were used to determine if there were optimal or pernicious environments for the reaction kinetics. The slag additives of TiO_2 powder and Al rod were used since they are commonly used to maintain the ingot chemistry and provide improved ingot quality. Finally, two slag chemistries of 60% CaF_2, 20% CaO plus 20% Al_2O_3 (60/20/20) and 70%CaF2 plus 30% Al_2O_3 (70/30) were used. All the melts except for the last used the 60/20/20 slag. The 70/30 slag composition was chosen to match the slag used on separate decontamination experiments conducted in Russia [9]. The first slag chemistry was recommended by the earlier work of Buckentin [1]. The range of surrogates, melting rates and differences are shown in Table VI. The difference column denotes when the TiO2 and Al additives were used along with the slag change for the last melt.

Melt	Surrogates	Melting Rate (units?)	Difference
1	CeO_2, HfO_2	0.8	
2	All	~3.0	
3	All	1.8-2.5	
4	All	1.0	TiO_2
5	All	2.3	TiO_2
6	All	1.0	
7	All	2.5	Al
8	All	2.4	70/30 Slag

Table VI: ESR Experimental Design

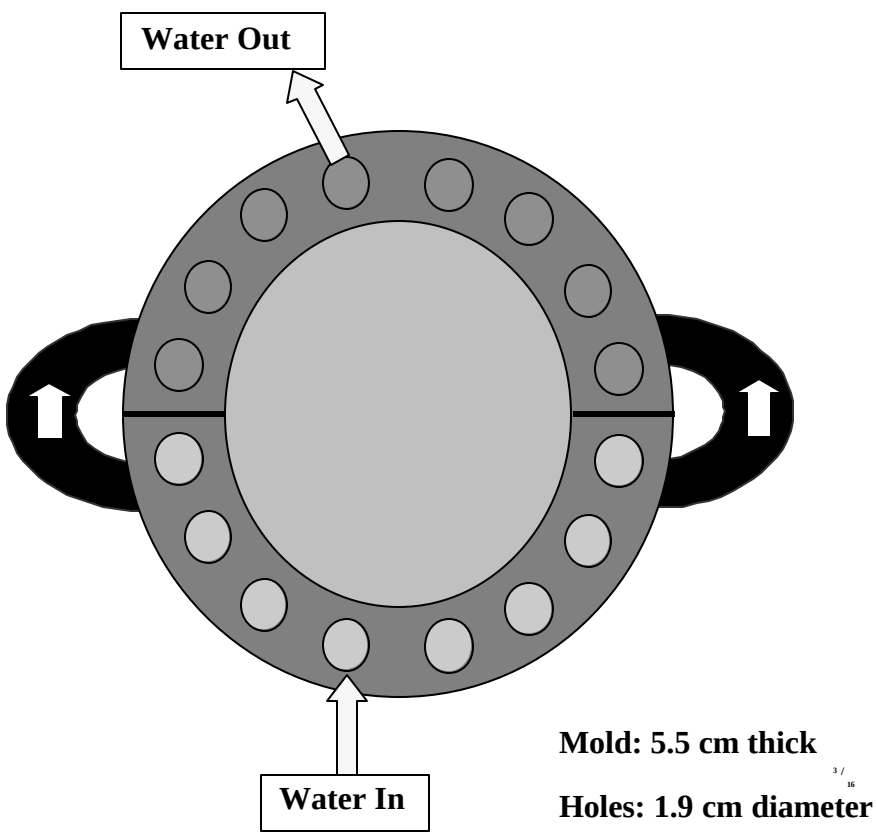

Figure 18: Top View of Split Mold

The melts used a specially designed vertically split mold (see Figure 18). When the mold was placed horizontally and the top half removed, the slag skin was left intact on

the surface of the ingot. Then after removing the ingot, the intact other half of the slag skin was available. This design allowed the slag skin to be sampled at regular intervals to observe any systematic or progressive changes that may have occurred during these melts. Two sets of pairs of Type-C thermocouples (TC's) were also used to monitor the slag temperature. With each pair, one was placed in a hole that was drilled at a 45° angle into the center of the electrode while the other was strapped to the side so the tips were in the same transverse plane.

D. Ingot Analysis

The ingots were sectioned and drill samples were taken at several locations. As an example, the locations for melt 4 are shown in Figure 19. Part A shows the locations

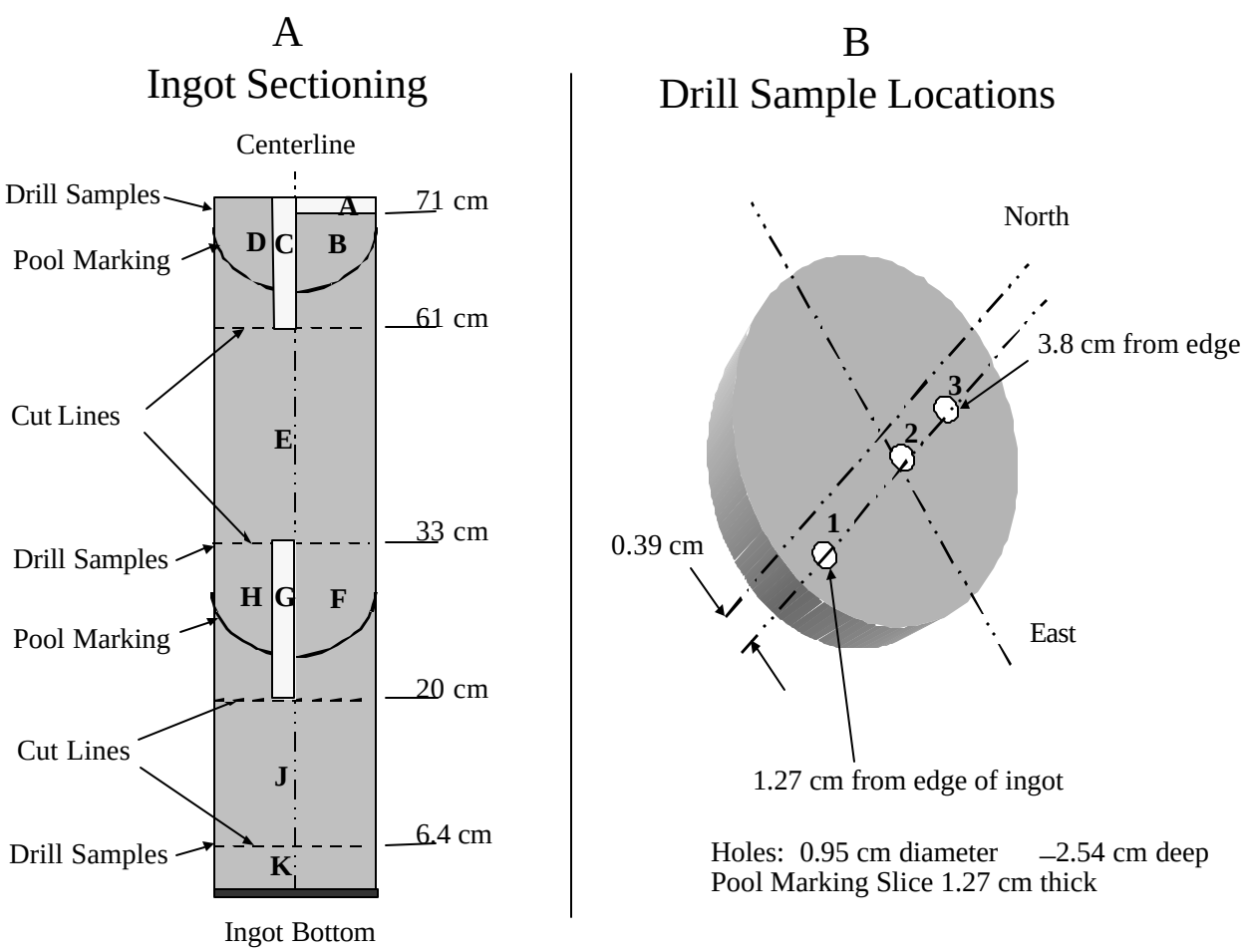

Figure 19: Melt 4 Ingot Cutting Map

where the slices were made and B identifies the locations of the drill samples. The locations were chosen to determine the horizontal and vertical distributions of the various compositional and surrogate elements throughout the ingot and to sample the areas where the TCs dissolved, i.e. where the HfO_2 was added to the melt. The horizontal locations

included a sample close to the bottom of the ingot and samples for all points where tungsten shot was used to mark the pool. Generally, the pools were marked about in the middle and near the top of the ingot, depending on when steady state conditions were achieved. The samples were not taken directly from the top but from about 1.2 cm below the surface to prevent slag contamination of the sample. The locations where the ingot was cut horizontally are designated by the dotted lines at 6.4 cm, 33 cm and 71 cm in the figure. At each horizontal location, three drill samples were taken 0.64 cm (0.25") from the center, at midradius, and at 1.2 cm (0.5") from the edge as shown in Part B of the figure. Approximately 13 grams of metal were taken from each location. The order of the sampling was randomized to minimize any systematic introduction of errors into the analysis. In addition to the drillings, longitudinal slices were taken so the pool profiles could be measured; these are marked as the rectangles G and C in Figure 19. All the pieces were stamped with the letter shown in the figure.

Initially, analysis of all the samples was performed on the ingots for a high melting rate, melt 3 and a low melting rate, melt 6. The pools for melt 3 were marked twice providing three vertical sampling regions, and melt 6, the pool was marked three times giving four regions. All the samples were analyzed to determine if there was any chemical variance from the middle to the edge and from the bottom to the top of the ingot. For comparison, drillings from the original electrode were analyzed as well. Duplicate samples were included for the top middle sections of both of the melts and of the electrode from melt 3, to characterize the variance in the analysis. The order for the analysis of the samples was randomized to prevent systematic errors from affecting the analysis. However, subsequent analysis did not show any systematic errors either as the samples were taken or during the analysis.

Melt 3

Sample	VLC*	HLC**	S ppm	Ce ppm	Cs ppm	Hf ppm	Re ppm	Sr ppm
1	E		250	0.2	<0.1	0.2	0.6	<0.1
2	E		250	0.2	<0.1	<0.1	0.4	<0.1
3	T	S	170	0.1	<0.1	0.2	57	<0.1
4	T	C	170	<0.1	<0.1	0.3	54	<0.1
5	T	C	160	0.2	<0.1	0.2	55	<0.1
6	T	MR	170	<0.1	<0.1	0.1	57	<0.1
7	M	S	42	0.2	<0.1	0.2	150	<0.1
8	M	C	84	0.1	<0.1	**31**	90	<0.1
9	M	MR	67	<0.1	<0.1	0.2	80	<0.1
10	B	S	25	<0.1	<0.1	<0.1	50	<0.1
11	B	C	31	<0.1	<0.1	**1.1**	46	<0.1
12	B	MR	42	**2.7**	<0.1	0.1	43	0.2

Melt6

Sample	VLC*	HLC**	S ppm	Ce ppm	Cs ppm	Hf ppm	Re ppm	Sr ppm
13	T	S	140	<0.1	<0.1	<0.1	49	<0.1
14	T	C	140	0.4	<0.1	<0.1	31	<0.1
15	T	C	140	0.3	<0.1	0.1	31	<0.1
16	T	MR	140	0.1	<0.1	0.1	41	<0.1
17	UM	C	120	0.1	<0.1	**1.5**	140	<0.1
18	UM	MR	120	0.1	<0.1	**0.7**	45	<0.1
19	LM	C	100	0.2	<0.1	0.3	130	<0.1
20	LM	MR	70	<0.1	<0.1	0.2	68	<0.1
21	B	S	38	0.1	<0.1	0.1	53	<0.1
22	B	MR	54	<0.1	<0.1	0.2	56	<0.1

***Vertical Code:** **T-Top, M-Middle, UM-Upper Middle, LM-Lower Middle, B-Bottom, E-Electrode**

**** Horizontal Code:** **S-Side, MR-Midradius, C-Center**

Table VII: Melt 3 and 6 Ingot Chemical Analysis

The relevant elemental ingot composition in parts per million (ppm) for the surrogate elements for melt 3 and 6 are given in Table VII. For a baseline, the chemical analysis of the original electrode for melt 3 is given at the top of the table. The rest of the table is arranged so that going up the ingot corresponds to going up the table. VLC and HLC are abbreviations for vertical location code (E-electrode, T-top, M-Middle, LM-lower middle, UM-upper middle, B-bottom) and horizontal location code (S-surface, MR-midradius, and C-center), respectively. These codes indicate the location in the ingot where the sample was taken based on the cut lines as shown in Figure 19. Values for samples 8 and 12 are displayed with a gray background because the readings are considered to be invalid since they were well outside the range of the expected value and other samples in the same region gave considerably different, more realistic values. Other values of interest discussed below are shown with darker border lines. The duplicate sample sets are samples 3 and 4 for melt 3 and 14 and 15 for melt 6. The data shown in the table were examined for patterns both across the ingot and along its length. A useful indicator in the vertical distribution and the slag capacity was the S content in the ingots. (Sulfur is a common contaminant in steels removed by ESR and a small quantity happened to be present in the electrodes used in these experiments.) The S content in both ingots gradually increased over the course of the melt. As the S was transferred from the metal to the slag, the slag's refining ability or holding capacity was gradually reduced. Consequently, the S content gradually increased in the ingot. Conversely, the refining capacity of the slag for the surrogates did not change over the course of the melt since the quantity of surrogates in the ingots remained relatively constant. Note that this was true even though the amount of surrogates considerably exceeded the quantity expected in actual decontamination melts. No consistent

differences or patterns between the center of the ingot and the midradius or surface locations were detected in the data. Consequently, the analysis of the remaining ingots was performed without investigating further for any horizontal variation.

The tabulated results for the chemical analysis of the ingots from melts 2, 5, 7 and 8 are shown in Table VIII. These melts were selected since they represented the full set of variations of melting conditions and chemistries, and provided the information about the interactions between the additives and slag compositions, and the surrogates. The information contained in melts 1 and 4 was supplied by the other melts, so they were not analyzed further. Also displayed in the table is the elemental analysis at the various ingot heights (column 2). Duplicate samples show the same heights. The shading in the table separates each melt. The values of particular interest are displayed in larger, bold type and will be discussed below.

The analysis of these melts revealed some variation in the effectiveness of the ESR process to transport the different surrogates from the liquid metal phase to the liquid flux. An insignificant amount of Re was detected in the original electrode, but from 50-150 ppm were detected in the ingot. This indicates that a significant percentage was retained in the ingot regardless of the melting conditions. Conversely, the amount of Cs and Sr in the ingot was consistently just at or below the detectable limit. Even though a much greater amount of Ce was added, its levels were at or usually below the values for the original electrode (Table VII) with the exception of the values from melts 5 and 7 highlighted with the bold borders. The top sample for melt 5 had a duplicate that did not show the increased value, while the other sample in melt 5 was at the bottom before much, if any, Ce would have been added. Consequently we believe those values are in error. However for melt 7 the higher Ce values appear to be valid. The Al deoxidizer impacted the reactions. The level of Hf increased as well. For the other melts, the level of Hf was again close to the detection limit with a few exceptions shown in Table VII and Table VIII with bold border lines (melt 3 sample 11, melt 6 samples 17 and 18, and one sample from melts 5 and 8). Since the Hf was not added gradually like the other surrogates, but was dumped into the slag in quantities of around 3-6 grams in a short period of time as the TCs melted, the test of the slag's kinetics and transport ability for Hf was more stringent. This procedure could have contributed to variability in the observed levels of Hf in the analysis, however the data is inconsistent. The samples for melts 5 and 8 were at the top well above the point where the TCs melted and the duplicate samples did not show increased levels of Hf. The sample for melt 3 was at the bottom before any TCs would have melted. That leaves the upper middle samples from melt 6. None of the other samples for that melt showed increased levels of Hf. Consequently we believe it is more likely that with these low concentrations of Hf, these values reflect the variability of the measurement process rather than showing an increase in the Hf. The final evidence for this hypothesis is presented in the next section with the slag analysis. The TiO_2 additive did not affect the decontamination, though an elevated level of Ti was seen for melt 5 (see Table VIII), particularly in the lower half when the TiO_2 concentration would have been the highest.

Melt	Ingot (cm)	S ppm	Ti%	Ce ppm	Cs ppm	Hf ppm	Re ppm	Sr ppm
2	34.93	86	0.010	<.01	0.1	<.01	1	<.01
2	34.93	79	0.010	0.1	0.2	0.2	120	<.01
2	0.00	300	0.010	<.01	0.1	<.01	0	<.01
5	71.12	250	0.018	0.1	0.1	0.1	69	<.01
5	71.12	230	0.019	**3.3**	0.3	**0.7**	67	<.01
5	30.48	120	0.038	<.01	0.1	0.2	84	<.01
5	6.35	54	0.073	<.01	0.1	<.01	61	<.01
5	0.00	250	0.010	**0.5**	0.3	0.1	1	<.01
7	63.50	140	0.010	**1**	0.2	**1.8**	69	<.01
7	63.50	120	0.010	**0.8**	0.1	**1.8**	70	<.01
7	53.34	110	0.010	**1.2**	0.1	**2.3**	74	<.01
7	6.35	42	0.010	0.2	0.2	0.2	110	<.01
8	72.06	290	0.010	0.1	0.1	**0.5**	73	<.01
8	72.06	300	0.010	0.1	0.1	0.1	73	<.01
8	55.88	330	0.010	<.01	0.1	0.2	94	<.01
8	6.35	200	0.010	<.01	0.1	<.01	65	<.01
8	0.00	310	0.010	<.01	0.1	<.01	2	<.01

Table VIII: Ingot Chemical Analysis for Melts 2,5,7 and 8

E. Slag Analysis

Slag samples were taken from the initial slag, the skin, and the cap (i.e. the slag that solidified on the top of the ingot when power was turned off). The initial slag gave the baseline values. The split mold was opened and the slag skin was sampled at regular intervals of the melt to determine if any slag chemistry changes during the melt. Also, the final composition of the slag caps was determined for the mass balance calculations. The results are shown in Table IX. The columns show the melt number, the location of the slag sample relative to the bottom of the ingot, and the measured amounts as percentages or ppm for the various elements. The location values of “I” indicate the initial slag sample while the values of “C” indicate the cap. Invalid values are marked with an “X”.

Since ~10 grams of Cs, Hf, Re and Sr were added and the slag quantity was 5 kg, if all the surrogate was transported to the slag, the expected concentration would be 0.2% or 2000 ppm. For the Ce, the concentration would be a factor of 10 greater at 2%. Typically, the relative quantity of the Ce, Hf and Sr surrogates increased, the higher up the ingot the slag sample was taken. Since the volume of slag remained essentially constant and these surrogates were added during the melt, that increase was expected as the slag retained those surrogates. Cs behaved differently. Its concentration was high very close to the bottom and then it dropped off, only to gradually increase as the melt progressed. Close to the bottom, the slag typically is significantly cooler since it has just been melted and may not have reached the operating temperature; also, the cooling from the bottom of the mold is still significant. It does appear that the Cs may preferentially solidify in the skin in this region. However, after the slag reached the typical melting temperature, the behavior of the Cs changed and the quantity in the skin decreased. Since the Cs was not found in the ingot and the quantity in the slag cap was less than 2000 ppm, some of it apparently volatilized at the higher temperature. The boiling points for Cs and CsF shown in Table V are considerably below the measured slag temperatures of 1800°C to 2150°C. Melt 8, however, did not show an increased level of Cs at the bottom of the slag. This slag, however, was not a pre-fused slag but simply a mixture of CaF_2 and Al_2O_3, so the melting characteristics were different. The quantity of Re in the slag remained relatively constant during the melts, since most of the Re was being transported to the ingot. An important factor was that the surrogates were detected in the slag skin. Therefore, in actual decontamination efforts, a high ingot surface quality is very important to minimize the possibilities for slag inclusions.

Since the quantity of Ce in the slag is approximately 2%, essentially all the Ce was transported to the slag, with the exception of melt 7 where only about 1% was detected. Since a concentration of 2% is a massive overtest, the slag clearly has sufficient capacity for normal decontamination operations. This is consistant with the results of the fundamental surrogate experiments at Boston University [16]. However for melt 7 with the Al addition, as noted previously, more Ce was detected in the metal. The mass balance for the metal and the slag do not completely account for all the Ce in this case, but both measurements indicate that the use of an oxidizer such as Al should be avoided for decontamination melts. For Hf, the detected quantity was approximately 0.2% except for melt 8 that was higher. Melt 8 used a different slag but it is not clear why the Hf was so high. The quantity for all the melts however indicates the slag successfully captured that surrogate, even though it was added in large amounts over short periods of time. This confirms the earlier arguments that the Hf values from the ingot analysis were likely in error. Very little Re was detected in the slag as expected since about 100 ppm was found in the metal samples. For Sr, however, none was found in the metal and less than half the expected quantity was detected in the slag. The amount of Cs detected was even less. Table V shows that the boiling point for Sr is below the measured slag temperatures but higher than Cs. Consequently both volatilized, and Sr volatilized at a slower rate than Cs. While the additions of the Al appeared to affect the reactions, the various melting rates and related slag temperatures and pool profiles had very little effect on the refinement.

Melt	Loc (cm)	Al%	Ca%	Ce%	Cs (ppm)	Hf%	Re (ppm)	Sr (ppm)
3	C	9.2	37.6	1.8	190	0.23	13	800
3	C	9.7	39.4	2.0	210	0.27	26	830
3	69	10.4	40.4	1.8	170	0.22	9	710
3	38	9.1	39.0	2.1	39	0.20	25	790
3	8	12.2	41.5	0.9	600	0.01	67	370
3	I	10.2	40.3	0.0	2	0.01	1	30
3	I	10.7	40.6	0.0	1	0.01	1	32
5	C	8.9	38.5	1.8	120	0.22	28	770
5	C	9.8	38.9	1.9	130	0.26	14	820
5	69	9.8	39.2	2.0	93	0.26	10	780
5	30	10.2	40.8	0.9	118	0.15	5	380
5	8	8.2	33.4	0.3	480	0.01	27	170
6	C	9.8	39.0	1.9	56	0.19	8	860
6	C	9.2	38.0	1.9	58	0.19	20	820
6	53	10.6	42.0	1.5	66	X	27	650
6	30	12.0	40.7	0.8	140	0.07	22	320
7	C	12.3	39.3	1.1	180	0.21	15	480
7	C	12.9	40.5	1.1	190	0.21	10	520
7	53	10.2	41.3	1.2	240	0.09	26	430
7	8	10.1	36.8	0.4	560	0.01	30	200
7	I	X	X	0.0	1	0.01	1	18
8	C	12.8	34.6	2.1	130	0.34	24	910
8	C	13.7	36.7	2.1	130	0.37	15	970
8	8	18.0	X	0.1	53	0.01	4	53
8	I	15.3	36.1	0.0	1	0.01	1	10

Table IX: Slag Chemical Analysis for Melts 3,5,6,7 and 8

F. Conclusions

Several experimental melts using surrogate elements, Ce, Cs, Hf, Re and Sr to simulate the reactions of several common radioactive contaminants, were conducted in an ESR furnace. The amount of the surrogates far exceeded the expected amounts of true decontamination melts. Even with these large amounts, the ESR process generally proved highly effective in keeping all the surrogates, except for Re, from the resulting stainless steel ingot, either by transporting them into the slag or by volatilization. The exception to this effectiveness was when Al was added as a deoxidizer. The levels of Ce and Hf in the

ingot for this case both showed elevated levels to about 1-2 ppm. Consequently, the use of Al or other oxidizers should be avoided for decontamination melts. The transport capacity did not seem to be affected by the addition of TiO_2 or by the different melting rates. The distribution of surrogates was found to be uniform on the transverse samples analyzed for both high and low melting rates. Consequently, the rates used should be selected to optimize the ingot surface quality minimizing the probabilities for slag inclusions. Generally, all the Re, Ce and Hf could be accounted for in the slag or in the metal except for Ce when Al rod was used. However, significant portions of the Cs and Sr were unaccounted for and were presumed to have volatilized. The Re was used as the chemical homologue for the important fission product, ^{99}Tc. Based on this study, ESR using the chosen slag compositions would not be appropriate for decontamination of technetium. However, all the surrogates for Pu and U were effectively transported from the metal, so the ESR can be recommended for decontamination of these elements.

3. ESR Experiments with Radionuclides

A project was funded at the Scientific Technology Center (STC), Mining & Chemical Combine (M&CC) (formerly K-26) in Krasnoyarsk, Russia, to melt surface-contaminated radioactive stainless steel piping. Initial work was supported by the International Proliferation Prevention Program to set up and test an ESR furnace to do test melt decontamination of stainless steel piping. This work described below was funded through this EMSP project to melt two pipe electrodes that were seeded with additional isotopes plutonium.

A. Contaminated Electrode Design and Fabrication

To fabricate consumable electrodes stainless pipes ranging from 12 to 134 mm in diameter and contaminated with radionuclides were taken out of the MCC solid waste storage. The pipes were selected to assemble an electrode by sequentially inserting tube into tube. After selecting the contaminated pipes, clean ones of the same dimensions were prepared to fabricate electrodes intended for preliminary melts to develop furnace operating procedures

The selected pipes were used to fabricate four (4) consumable electrodes: two of contaminated and two of clean tubes. Each electrode had a weight of about 300 kg. Figure 20 shows the electrode dimensions.

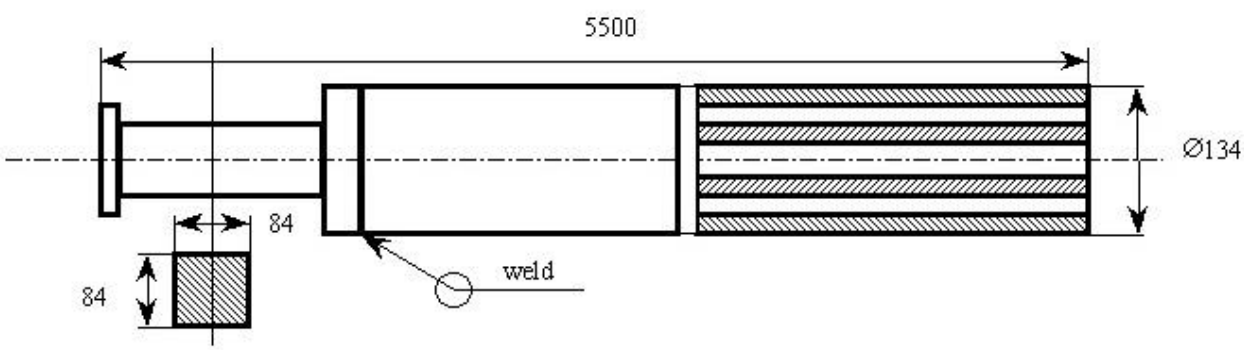

Figure 20: Electrode Fabrication and Dimensions

Segments to determine a content of radioactive isotopes were selected from the contaminated pipes. Table X gives a measured initial contamination of the stainless steel pipes. Data given in Table X are approximate since it's not possible to determine a real content of radionuclides due to a complexity of the analysis and non-uniformity of the contamination distribution over the pipe surfaces. Pipes of small diameters (12, 18, 32 mm) were not subject to analysis for radionuclide content.

Item	*Pipe Diameter mm*	*Activity, Bq per sample*							
		Pu^{239}	Am^{241}	Cs^{134}	Cs^{137}	Eu^{152}	Nb^{94}	Co^{60}	Ce^{144}
1.	57	-	-	-	9	-	-	-	-
2.	64	-	-	-	46	-	-	58	-
3.	75	-	-	-	678	-	-	57	-
4.	84	-	-	-	27	-	-	-	-
5.	134	-	-	-	9	-	-	-	-

Table X: Contaminated Steel Isotopic Content Prior to Purification

In order to more accurately estimate a distribution of Pu^{239} when melting, a known amount of plutonium (12 mg) was additionally inserted into each contaminated electrode. The following was the procedure for adding the Pu:

- treatment of inner surface of a thin-walled stainless tube with concentrated nitric acid with heating up to 400-500°C to provoke an intercrystalline corrosion;
- insertion of a calculated amount of the Pu^{239} standard solution;
- de-nitration and baking of plutonium dioxide by heating in vacuum;
- welding of the tube inside a consumable electrode.

Table XI gives the nominal content of the contaminated steel alloy.

Steel Type	*Content, %*							
	C	Si	Mn	Cr	Ni	Ti	S	P
12C18N10T	≤0.12	≤0.8	≤2	17÷19	9÷11	0.6÷0.8	≤0.02	≤0.035

Table XI: Alloy Content of the Contaminated Steel Pipes

B. Selection of the Refining Slag

In ESR, the slag layer serves as a primary heat source and purifies the metal of radioactive contamination. If the slag's electrical resistance at a specified operating temperature is not sufficient, it is very hard or even impossible to have the remelt conditions satisfactory. If the slag's chemical activity is not sufficient, it fails to achieve the required level of purification. If the slag has a high chemical activity then in re-melting the alloying elements which should be kept or remain in the metal will be taken out into the slag. The slag performs some other functions. Solidifying on the mold walls, it prevents the melted metal from contacting with the walls thus isolating the metal the mold both electrically and thermally from the electrode melted metal and promotes forming a smooth ingot surface.

It should be taken into consideration that radionuclides on contaminated pipes are in the oxidized form and basically located in superficial layers due to corrosion of the metal. Therefore, one of the main factors which affects the steel purification by ESR is a quality with which the slag separates from the ingot metal and ability of removing non-metallic inclusions from the metal. Based on experience, the following slags are the most acceptable: Slag No. 77 (56.7% CaF_2 + 15% CaO + 28.3% Al_2O_3), Slag No. 79 (63.% CaF_2 + 18.3% CaO + 18.3% Al_2O_3), Slag No. 91 (70% CaF_2 + 10% CaO + 20% Al_2O_3), and ANF6 (70% CaF_2 + 30% Al_2O_3). For these melts on both clear and contaminated pipes, the two refining slags used were No. 77 and ANF6.

The slag No. 77 was produced in an arc furnace by melting original components over an iron metallic liquid pool and grinding with a jaw grinder up to a required size of the grain. The ANF6 slag was purchased. Prior to use the slags were baked out in a muffle furnace at a temperature of 850°C for three (3) hours. After baking the slags were placed in a sealed container to protect from moisture.

C. Melting and Sampling Procedure

The melting procedures were first developed on clean electrodes. Two melts on clean electrodes with slags No. 77 and ANF6 were carried out. For melt start-up, the power was manually controlled for 10-15 min., then the process was switched to automatic control. After melting 95% of the electrode mass, the process went back to manual control, and electrical power was gradually decreased to bring up the shrinkage. Thirty minutes after completing the process and cooling, the slag the mold were lifted, the slag crust was separated from the ingot, the ingot surface was subjected to mechanical cleaning. It was noted that the ingot No. 1 (slag ANF-6) surface was shiny without slag inclusions to be seen. The ingot No.2 had a matt surface with multiple slag inclusions up to 1 mm in depth.

Experiments on the "clean" electrode showed that an amount of slag required for a stable ESR process is at least 10 kg. Otherwise, there is unstable operation of the power transformer when supplying power to the slag pool. Two (2) ingots resulted from the re-melting of clean electrodes had a fully dense structure typical for the ESR-produced ingots. However, the ingot produced with the use of slag No. 77 contained in the bottom part some insignificant inclusions of the slag, and the slag crust was harder to separate from the ingot.

Subsequent to that, the ESR process was carried out with contaminated electrodes. Table XII provides primary parameters of the remelt. In remelting, the air from the ventilation system and operating room were sampled to analyze the content of radionuclides in it.

Item	Parameter	Unit	Value	Comments
INGOT NO.1 (ANF-6 SLAG)				
MANUAL MODE				
1.	Amperage	KA	up to 6	
2.	Voltage	V	44	
3.	Slag Pool Depth	m	0.12	
4.	Slag Quantity	kg	12	
5.	Metal Pool Depth	m	0.03÷0,04	
AUTOMATIC MODE				
1.	Amperage	kA	4.5	
2.	Voltage	V	44	
3.	Slag Pool Depth	m	0.12	
4.	Slag Quantity	kg	12	
5.	Metal Pool Depth	m	0.03÷0.04	
Ingot No. 2 (Slag No. 77)				
MANUAL MODE				
1.	Amperage	KA	up to 6	
2.	Voltage	V	44	
3.	Slag Pool Depth	m	0.1	
4.	Slag Quantity	kg	10	
5.	Metal Pool Depth	m	0.04	
AUTOMATIC MODE				
1.	Amperage	KA	4.3	
2.	Voltage	V	44	
3.	Slag Pool Depth	m	0.1	
4.	Slag Quantity	kg	10	
5.	Metal Pool Depth	m	0.04	

Table XII: Contaminated Steel Remelting Primary Parameters

Ingots cleaned of the slag and superficial contamination with by etching for two hours with a solution containing three volumetric parts of H_2SO_4, one part of HNO_3 and 50 g/l of NaF were mechanically cut up. Three cylinder-like samples (hereafter the "pucks") were cut out of the ingot No.1 (see Figure 21) and than the pucks were cut for samples to be subjected to mechanical and corrosion testing, for research of the microstructure (see Figure 22) and for determination of the isotopic content. One puck was cut out of the middle part of the ingot No. 2.

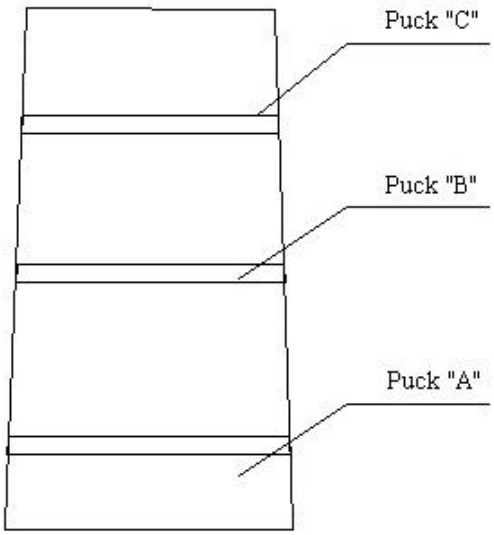

Figure 21: Ingot No. 1 Cutting Plan

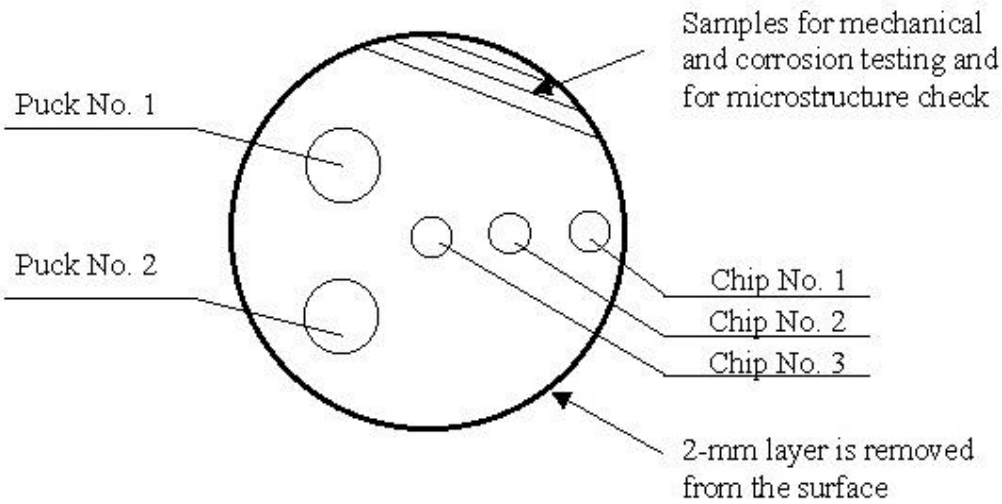

Figure 22: Chips for Analysis and Samples for Mechanical Testing and Radioactivity Measurements

D. Analytical Techniques

A content of radionuclides in original and purified steel, and in the contaminated slag was determined with SBS-50 gamma-spectrum analyzer with HpGe GC4520 detector and by alpha-spectrometer technique with SBS-50m-2 spectrum analyzer with DKPS-500 detector. To determine a content of Pu-239 a sample was inserted with a mark of standard solution of Pu-238 to identify Pu-239. An error of the technique is determined with a statistical error of determining the Pu^{239} pick-to- Pu^{238} pick ratio in alpha spectrum and indicated for each measurement. A micro-content of initial and purified steel was analyzed according to standard techniques of nuclear-absorption spectrometry with the use of AAS-3 spectrum analyzer.

Mechanical properties of the purified metal were determined by static tension on a mechanical test machine with plotting the sample tension pattern. The tests were carried out on 10×5×150 mm samples. Based on the tests results the steel ultimate strength, yield strength and elongation were determined.

A propensity of the purified metal to inter-crystalline corrosion (ICC) was researched with two methods:

- under conditions corresponding to Schtraus method (with plotting a polarization curve in a solution of chlorine acid with sodium chloride);
- with boiling in 65% solution of nitric acid for 48 hours with subsequent determination of corrosion rate resulted from a depth the ICC has reached on a metallurgical specimen. A propensity of the metal to ICC with Schtraus method was judged by a pick in anode current within potentials ranging plus 50 through plus 500 mV relative to the chloride -silver electrode to compare.

E. Discussion of the Results

Table XIII gives results of analytical determination of a content of radionuclides in purified steel and in used slags.

Item	Sample Name		Radionuclide Activity, Bq/kg					
			Pu^{239}	Am^{241}	Cs^{137}	Co^{60}	Nb^{94}	Eu^{152}
Ingot No. 1								
1.	Puck “C”	chip No. 1	220 (120)	-	-	-	-	-
		chip No. 2	320 (160)	-	-	-	-	
		chip No. 3	99 (64)	-	-	-	-	-
		layer from the surface	300 (300)	-	-	-	-	-
		puck No. 1	-	-	-	33.41	3.58	-
		puck No. 2	-	-	-	30.024	2.54	
2.	Puck “B”	chip No. 1	330 (330)	-*	-	-	-	-
		chip No. 2	250 (150)	-	-	-	-	
		chip No. 3	224 (90)	-	-	-	-	-
		layer from surface	712 (220)	-	-	-	-	-
		puck No. 1	-	-	-	95.80	6.4	-
		puck No. 2	-	-	-	93.95	7.4	
3.	Puck “A”	chip No. 1	780 (230)	-	-	-	-	-
		chip No. 2	1870(590)	-	-	-	-	
		chip No. 3	752 (180)	-	-	-	-	-
		layer from surface	2000(400)	-	-	-	-	-
		puck No. 1	-	694.3819	-	21.95	3.16	-
		puck No. 2	-	906.693	-	19.75	3.75	
4.	Slag ANF-6		3445200 - 2246303; 1.32 mg/kg	345298.7	249.1654	69.77	-	234.5

continuation of Table XIII

Itm	Sample's Name		Radionuclide Activity, Bq/kg					
			Pu^{239}	Am^{241}	Cs^{137}	Co^{60}	Nb^{94}	Eu^{152}
Ingot No. 2								
1.	Puck "B"	chip No. 1	75 (49)	-*	-	-	-	-
		chip No. 2	99 (10)	-	112.76	-	-	
		chip No. 3	192 (42)	-	-	-	-	-
		layer from the surface	176 (96)	542.4	848.64	-	-	-
		puck No. 1	-	363.68	-	29.90	1.87	-
		puck No. 2	-	341.92	-	31.39	1.9	
2.	Slag No. 77		2763586.8; 1.23 mg/kg	735852.6	103.005	10.68		

Note: Indicated in brackets is an error of measurements; "-" – not detected.

Table XIII: Analytical Chemistry Results

Table XIV provides results of the purified metal analysis.

Item	Sample Name		Content, %							
			Mn	Ni	Cr	P	Ti	Si	C	S
Ingot No. 1										
1	Puck "A"	chip No. 1	0.89	10.34	18.33	0.03	0.19	0.41	0.084	0.006
		chip No. 2	0.97	9.92	18.26	0.028	0.21	0.39	0.066	0.004
		chip No. 3	0.97	10.43	18.37	0.031	0.22	0.43	0.08	0.005
2	Puck "B"	chip No. 1	0.94	10.20	18.31	0.023	0.27	0.38	0.076	0.006
		chip No. 2	0.98	9.99	18.28	0.026	0.33	0.39	0.07	0.007
		chip No. 3	1.08	10.11	18.10	0.031	0.28	0.37	0.071	0.006
3	Puck "C"	chip No. 1	1.06	10.24	18.55	0.030	0.23	0.38	0.064	0.010
		chip No. 2	1.01	11.02	19.47	0.032	0.30	0.39	0.072	0.009
		chip No. 3	1.02	11.00	18.3	0.027	0.31	0.38	0.082	0.010

Continuation of Table XIV

Item	Sample Name		Content, %							
			Mn	Ni	Cr	P	Ti	Si	C	S
Ingot No. 2										
4	Puck "B"	chip No. 1	1.07	10.80	18.18	0.025	0.12	0.39	0.080	0.005
		chip No. 2	1.07	10.45	17.73	0.024	0.16	0.45	0.078	0.005
		chip No. 3	1.06	10.17	16.91	0.025	0.13	0.44	0.075	0.004
		layer from the surface	1.10	10.56	17.10	0.031	0.12	0.32	0.070	0.005

Table XIV: Purified Steel Chemical Analysis

The analysis of the data given in Tables XIII and XIV shows that both ingots have, by and large, a uniform distribution of both residual radionuclides and the steel macro-components. The purified steel has a reduced content of titanium relative to the original steel (12C18N10T, the USA analogue is steel 321 per AISI). The chemical compound of the remelted steel corresponds to those of 08C18N10 steel (the USA analogue is steel 302 per AISI). It should be noted that the ESR reduces the sulphur content in the steel 2 to 4 times and with the slag No. 77 remelt a purification of sulphur twice those did with the slag ANF-6. It has been noted a 50% reduction, on the average, in carbon content. The middle and upper part of ingot No.1 and middle part of ingot No.2 were the most clean in radionuclides (Pu^{239}, Co^{60}, $Nb^{94,95}$). The second ingot has a little higher content of americium-241 than the middle part of ingot No. 1 does. It is probably associated with not sufficiently full removal of slag inclusions when re-melted with slag No. 77.

Based on the data obtained the stainless steel purification factor K_{prf} and the slag-metal system radionuclide distribution factor K_d are

$$K_{prf} = C_{cnt} / C_{prf} ,$$

where: C_{cnt} – concentration of radionuclides in contaminated steel, % mass;

C_{prf} – concentration of radionuclides in purified steel, % mass.

$$K_d = C_{slag} / C_{prf} ,$$

where: C_{slag} – concentration of radionuclide in the slag after purification, % mass.

The steel purification factors produced in ingot No.1 are:

For Puck "C":

K_{prf}^{Pu239} = 158 to 489
K_{prf}^{Am241} > 10000
K_{prf}^{Cs137} > 250
K_{prf}^{Co60} ~ 2
K_{prf}^{Eu152} > 1000

A total residual radioactivity in alpha emitters is ~ $(2.6\text{-}8.6)\cdot 10^{-9}$ Ci/kg;
In gamma emitters it equals < $0.1\cdot 10^{-9}$ Ci/kg (< $3.48\cdot 10^{-7}$ mg·ekV·Ra/kg).

Puck "B":

K_{prf}^{Pu239} = 220 to 642
K_{prf}^{Am241} > 5000
K_{prf}^{Cs137} > 150
K_{prf}^{Co60} – no purification
K_{prf}^{Eu152} > 1000

A total residual radioactivity in alpha emitters is ~ $(0.6 \text{ to } 1.9)\cdot 10^{-8}$ Ci/kg;
In gamma emitters it is equal to < $0.3\cdot 10^{-9}$ Ci/kg (< $1\cdot 10^{-7}$ mg·ekV·Ra/kg).

Puck "A":

K_{prf}^{Pu239} = 84 to208
K_{prf}^{Am241} > 300
K_{prf}^{Cs137} > 200
K_{prf}^{Co60} ~ 2
K_{prf}^{Eu152} > 1000

The total residual radioactivity in alpha emitters is ~ $(2 \text{ to } 5.4)\cdot 10^{-8}$ Ci/kg;
In gamma emitters it is equal to < $0.15\cdot 10^{-9}$ Ci/kg (< $2.3\cdot 10^{-8}$ mg·ekV·Ra/kg).
The Pu^{239} distribution factor (slag-metal, mass%) is:

K_d = 20671 to 417600.

The steel purification factor in producing Ingot No. 2:

Puck "B":

K_{prf}^{Pu239} = 815 to 1582
K_{prf}^{Am241} > 900
K_{prf}^{Cs137} - (not determined due to slag inclusions in chips)
K_{prf}^{Co60} ~ 2
K_{prf}^{Eu152} > 1000

A total residual radioactivity in alpha emitters is ~ (2.67 to 8.6)·10^{-9} Ci/kg, in gamma emitters it equals < 1·10^{-8} Ci/kg (< 3.48·10^{-5} mg·ekV·Ra/kg).

The Pu^{239} distribution factor (slag-metal, mass%) in producing Ingot No. 2 is:

K_d = 32427 to 10032.

An analysis of the gas release samples has show that at the beginning of the ingot No. 2 remelting some increase in a content of plutonium relative to the ingot No. 1 melting took place (up to 15 Bq/m^3 vs. 1 Bq/m^3). Notwithstanding that thermodynamic calculations deny a probability of composition of volatile compounds of plutonium and uranium (such as UF_6 and PuF_6), volatile compounds of uranium and plutonium are formed by the following reactions:

$$CaF_2 + H_2O \rightarrow CaO + 2HF;$$

$$12HF + 2U(Pu)O_2 + O_2 \rightarrow 2UF_6\ (PuF_6) + 6H_2O.$$

Resulting reaction: $6CaF_2 + 2U(Pu)O_2 + O_2 \rightarrow 6CaO + 2UF_6\ (PuF_6)$, in which water serves as catalyst. It is known that CaO-containing slags are more hygroscopic than CaF_2 + Al_2O_3-containing slags, which is why in remelting with slag No. 77 a lot of plutonium released into a gaseous phase.

F. Conclusions

The Mining and Chemical Combine in cooperation with Sandia National Laboratories has produced a pilot furnace facility for deactivation of stainless steel with electroslag remelting (ESR). The facility allows deactivation of cylinder-shaped electrodes of contaminated steel up to 134 mm in diameter and up to 300 kg in weight.

The ESR facility was involved in remelting two contaminated electrodes assembled of stainless pipes (steel 12C18N10T which the USA analogue is Type 321 stainless steel) with the use of two (2) refining slags:

- 70 %CaF_2 + 30 % Al_2O_3 (Slag No. 77);
- 56.7 % CaF_2 + 15 % CaO + 28.3 % Al_2O_3 (ANF-6).

It has been shown that the ESR results in stainless steel deactivation of plutonium-239, cesium-137, americium-241 and europium-152 with high purification factors. At the same time, a purification of such radionuclides as cobalt-60 and niobium-94 practically does not occur.

The purified stainless steel is high quality with a uniform distribution of residual contaminations and main alloying components of the steel; satisfactory structural and mechanical properties; and absence of defects and inclusions especially when re-melted with the slag 70 %CaF_2 + 30 % Al_2O_3. The product could be reused as steel 08C18N10 (the USA analogue is steel 302 per AISI) to fabricate equipment utilized in radiochemical and general industrial production if not welded or, if welded, with subsequent thermal treatment of the welds. Utilization of a purified steel in strong oxidizing environments

(such as concentrated solutions of nitric acid) is allowable only after subjecting it to extra alloying with titanium or niobium.

Slag inclusions in the ingot when re-melted with the 56.7 % CaF_2 + 15 % CaO + 28.3 % Al_2O_3 slag at the beginning of the re-melting indicate that the re-melting mode for this particular slag is not optimal. With further researches this drawback may be eliminated. Unlike ingot No.1, the surface of ingot No.2 containing slag inclusions requires carrying out extra treatment of the surface (scalping and etching) prior to subsequent usage.

It has been noted that an increased release of plutonium to the gaseous phase at the beginning of re-melting with slag No. 77 in comparison with slag ANF-6 is probably associated with a formation of such volatile compounds of plutonium as PuF_6 with water vapor, which is contained in more hygroscopic slag No. 77.

For industrial scale decontamination melting, a first melt furnace to produce consumable electrodes for ESR is necessary. This facility could be an arc, plasma, or induction furnace with a unit for pouring metal into an ingot mold of the required geometry. For simplicity and safety, preference should be given to a small capacity plasma-arc furnace (up to 300 kg).

Other slag systems for steel deactivation with ESR need to be studied. These systems are 45 %CaO + 45 % Al_2O_3 + 10 % MgO; 43 % CaO + 43 % Al_2O_3 + 14 % $Na_2B_4O_7$; 38 % CaO + 38 % Al_2O_3 + 10 % MgO + 14 % $Na_2B_4O_7$, etc. and which can be used for ESR of stainless steels. Use of thes slags in ESR would allow recycling of lining materials (spent crucibles) contaminated in using the first melt furnace.

IV. Relevance, Impact, and Technology Transfer

This project investigated in detail the Electroslag Remelting (ESR) process as a potential method to volumetrically decontaminate metal waste. ESR was shown to be effectively remove several surrogate compounds selected to chemically mimic actual contaminates. Experiments at STC in Russia demonstrated efficient removal of several, but not all, radionuclides introduced in the experiments. These results demonstrate that ESR melting could be a useful process for volumetric metal decontamination.

Our Russian colleagues also performed an engineering design study for a complete melt decontamination facility. Their recommendation was to utilize ESR as a final melting step to decontaminate and cast high quality ingots. They also recognized the need to do a first step consolidation/decontamination melt, using another process, to be able to handle the range of geometries of scrap forms. Ingots produced in the first consolidation melt would then be remelted by ESR. This would provide a dual cleanup process with two different slag chemistries, which could be optimized for overall effect. They are pursuing this recycling technology.

In the US, it has been difficult to move this work on to a demonstration stage. Results were presented at several conferences, workshops, and DOE site visits. Two major factors have limited its progress. First, the cost to do a demonstration would be high in the US, estimated at several $M, and it is difficult to fund decontamination demonstration projects at that level. Second, there is strong public opposition to any possibility of decontaminated metal entering general use. For this technology to be applied, the DOE would be the only potential customer for the product, possibly for use as radioactive waste shipping or storage containers and components. Substitution of decontaminated alloys for these applications would reduce procurement costs and eventual disposal costs.

V. Project Productivity

The project met its goals to optimize the ESR melt decontamination process by developing a basic understanding of the factors which govern the partitioning of various radionuclides between the metal, slag, and gas phases. The original plan was revised mid way through the project when the opportunity became available to conduct ESR experiments at the Scientific Technology Center in Zheleznogorsk, Russia using radioactive dopant compounds. This allowed us to compare the behaviors of both the radioactive species and the surrogate compounds selected to mimic them.

VI. Personnel Supported/Associated

Dr. James A. Van Den Avyle, SNL
Dr. David Melgaard, SNL
Dr. Martin Molecke, SNL
Dr. M. Eric Schlienger, SNL,
Greg J. Shelmidine, SNL
Dr. James Stepanek, SNL
Dr. Rodney Williamson, SNL
Prof. Uday Pal, Boston Univ.

E. Chiang, Boston Univ.
Dr. Kuo-Chih Chou, Boston Univ.
W. P. Chernicoff, Boston Univ.
C. J. MacDonald, Boston Univ.
D. Woolley, Boston Univ.
T. Keenan, Boston Univ.
A. Krishnan, Boston Univ.
Dr. Sergie I. Bychkov, STC-M&CC
Dr. K. G. Kudinov, STC-M&CC
Dr. Sergie Podoynitsin, STC-M&CC
Dr. Vasily V. Zhidkov, STC-M&CC

VII. Publications

Eric Schlienger, Joe Michael, James Van Den Avyle, David Melgaard, Greg Shelmidine, "Solidification Sequence as a Means of Containing Radionuclides During Melt Decontamination", International Conference on Incineration and Thermal Treatment Technologies, Salt Lake City, May 11-15, 1998.

D. K. Melgaard, G. J. Shelmidine, "ESR Process Instabilities while Melting Pipe Electrodes", Liquid Metal Processing and Casting, Vacuum Metallurgy Division, American Vacuum Society, Santa Fe, NM, February 21-24, 1999, pp 176-186.

W. P. Chernicoff, C. J. MacDonald, H. Gao, D. Woolley, K. C. Chou, U. B. Pal, J. Van Den Avyle and M. A. Molecke, "Electroslag Remelting (ESR) Slags for Removal of Radioactive Oxide Contaminates from Stainless Steel",

Uday B. Pal, "Electroslag Remelting (ESR) Slags for Removal of Radioactive Oxide Contaminants from Stainless Steel," Sandia Report, SAND99-2082, August 1999.

U. B. Pal, C. J. MacDonald, E. Chiang, W. C. Chernicoff, K. C. Chou, J. Van Den Avyle, M. A. Molecke, and D. Melgaard, "Behavior of Ceria as an Actinide Surrogate in Electroslag Remelting and Refining Slags," Metallurgical and Materials Transactions, 32B, December 2001, p. 1119.

D. K. Melgaard, G. J. Shelmidine, J. A. Van Den Avyle, and M. A. Molecke, "Radionuclide Surrogate Decontamination of Metal using Electroslag Remelting", EPD Congress 2003, M. Schlesinger, ed., TMS (The Minerals, Metals & Materials Society, 2003 (in-press).

Masters Theses:

C.J. McDonald, "Calibration-Free Electrical Conductivity Measurements for Highly Conductive Slags," MS Thesis, Boston University, Department of Manufacturing Engineering, January 2000.

W. C. Chernikoff, "Decontamination of Radioactive Stainless Steel in the Electroslag Remelting Process," MS Thesis, Boston University, Department of Manufacturing Engineering, January 2001.

VIII. Interactions

Workshops:

J. A. Van Den Avyle, DOE EMSP National Workshop, Chicago, IL, July 27-29, 1998.

J. Van Den Avyle, E. Schlienger, D. Melgaard, J. Stepanek, G. Shelmidine, U. Pal, W. Chernicoff, "Optimization of Factors Governing the Partitioning of Radionuclides during Melt Decontamination of Stainless Steels", EMSP Workshop, U.S. DOE Environmental Management Science Program, Oak ridge, TN, September 22, 1998.

J. A. Van Den Avyle, DOE EMSP D&D Workshop, Savannah River Technology Center, November 17-18, 1998

J. A. Van Den Avyle, D. K. Melgaard, and R. L. Williamson, "Melt Decontamination of Radioactively Contaminated Stainless Steel Project #60363", EMSP National Workshop, U.S. DOE Environmental Management Science Program, Atlanta, GA April 24-27, 2000

Presentations:

W. P. Chernicoff, C. J. MacDonald and U. B. Pal, "Electroslag Remelting (ESR) Slags for Removal of Radioactive Oxide Contaminants from Stainless Steel," Global Symposium on Recycling, Waste Treatment and Clean Technology, San Sebastian, Spain, TMS, (1999), p. 803.

Eric Schlienger, Joe Michael, James Van Den Avyle, David Melgaard, Greg Shelmidine, "Solidification Sequence as a Means of Containing Radionuclides During Melt Decontamination", International Conference on Incineration and Thermal Treatment Technologies, Salt Lake City, May 11-15, 1998.

D. K. Melgaard, G. J. Shelmidine, "ESR Process Instabilities while Melting Pipe Electrodes", Liquid Metal Processing and Casting, Vacuum Metallurgy Division, American Vacuum Society, Santa Fe, NM, February 21-24, 1999, pp 176-186.

D. K. Melgaard, G. J. Shelmidine, J. A. Van Den Avyle, and M. A. Molecke, "Radionuclide Surrogate Decontamination of Metal using Electroslag Remelting", EPD Congress 2003, M. Schlesinger, ed., TMS (The Minerals, Metals & Materials Society), 2003.

J. A. Van Den Avyle, M.A. Molecke, R.L. Williamson, D. K. Melgaard, U.B. Pal, W.P.

Chernicoff, and C.J. MacDonald, S.I. Bychkov, S. Podoynitsin, and K.G. Kudinov, "Electroslag Remelting Porcess Studies for Decontamination of Stainless Steels: Current Results" Poster Presentation at the American Chemical Society Division of Nuclear Chemistry and Technology, First Accomplishments of U.S. DOE Environmental Management Science Program, New Orleans, LA, August 22-26, 1999.

IX. Transitions

At this time, we are not aware that other facilities in the US are utilizing the technologies or process developed in this program. Proposals in recent years to decontaminate and recycle metal scrap (e.g. nickel at Y-12) have met with strong resistance from the general public as well as the metals recycling industry.

X. Patents

None

XI. Future Work

The experimental work and analyses of the results of this EMSP program are complete, and no follow-on efforts are currently planned at Sandia or at Boston University. Project participants at the Scientific Technology Center, Mining & Chemical Combine in Russia continue to be interested in applying this technology toward recycling radioactive contaminated metal waste in Russia.

XII. Literature Cited

1. J. M. R. Buckentin "Melt Decontamination of Radioactive Stainless Steel by Electroslag Remelting", PhD Thesis, Oregon Graduate Institute of Science & Technology, Materials Science Department, March 1996.
2. S.A. Worcester, L.G. Twidell, D. Webber, D.J. Paolini, T.A. and Weldon, "Report on Decontamination and Decarburization of Stainless Steel and Carbon Steel by Melt Refining," Prepared for Lockheed Idaho Technologies Company Under Subcontract No. C85-110767 and the U.S. Department of Energy.
3. M. Choudhary and J. Szekeley: Metallurgical and Materials Transactions B, 1981, 12B, pp.418-421.
4. S.A. Worcester, L.G. Twidell, D.J. Paolini, T.A. Weldon and R.E. Mizia, "Decontamination of Metals by Melt Refining/Slagging," WINCO-1198, Prepared for the U.S. Department of Energy, Idaho Field Office, March 1994.
5. E.M. Levin, C.R. Robbins and H.F. McMurdie, "Phase Diagrams for Ceramists Vol.1," Edited by M.K. Reser, Published by the American Ceramic Society, Columbus, Ohio, 1964.
6. C.J McDonald, "MS Thesis in Manufacturing Engineering-Calibration-Free Electrical Conductivity Measurements for Highly Conductive Slags," Boston University, January 2000.
7. V.D. Eisenhüttenleute: Slag Atlas, Verlag Stahleisen m.b.H., Düsseldorf, Germany, 1981, pp. 258-282.
8. W. E. Duckworth and G. Hoyle, Electroslag Refining (London: Chapmand and Hall Ltd, 1969).
9. A. Mitchell, "Electroslag and Vaccum Arc Remelting Processes, "Electric Furnace Steelmaking, (Publication Iron and Steel Society / AIME 1985), 191-236.
10. D.K. Melgaard and R.L. Williamson, "Control of Remelting Processes for Superalloys and Aerospace Titanium Alloys, Journal of Minerals Metals & Materials Society, 50 (3) (1998), 13-17.
11. K.C. Mills and J.S. Powell, "The Physicochemical Properties of Slags," (NPL Report Chemistry, 103 (11), 1976).
12. A. Mitchell, "The Chemistry of ESR Slags, "Canadian Metallurgical Quarterly, 20 (1) (1981), 101-112.
13. S.F. Medina and M.P. de Andres, "Electrical Field in the Resistivity Medium (slag) of the ESR process: influence on ingot production and quality", Institute of Metals, (Feb. 1987), 110-121.
14. Kitagawa, K., Nagura, K., and Noura, T., "Treatment of Radioactive Metallic Waste by the Electro-slag Melting Method," Kobe Steel Engineering Reports, Vol. 33, No. 1, (Jan. 1983),1-6.
15. Ochiai, A., Kitagawa, K., Sawada, Y., Isuhara, S., and Ohtsuka, K., "Treatment of Plutonium-Contrminated Metallic Waste by the Electro-slag Melting Method," IAEA-SM-261/20;EDB-84-020441, Japan: Kobe Steel, (June 1982).
16. U.B. Pal, C.J. MacDonald, E. Chiang, W.C.Chernicoff, K.C. Chou, J.A. Van Den Avyle, M.A. Molecke and D.K. Melgaard, "Behavior of ceria as an actinide surrogate

in electroslag remelting and refining slags", Metallurgical and Materials Transactions B-Process Metallurgy and Materials Processing Science 32 (6) (Dec 2001) 1119-1128.